Centre for
Advanced 2D Materials

Nature of Interactions between Single-Stranded DNA Molecules and Graphene Substrate through Atomic Force Microscope

Nanotechnologies for ICTs - Master Thesis - a.a 2019/2020

Author: *Elia Alberti*

Supervisors:

Prof. Matteo Cocuzza (Polito)

Prof. Slaven Garaj (NUS)

Dr. Milan Blaskovic (NUS)

Co-Supervisors:

Prof. Giancarlo Canavese (Polito)

POLITECNICO
DI TORINO

Contents

Abstract

During this thesis project research, there were collected experimental data regarding interactions of individual DNA molecules with monolayer graphene and develop breakthrough model to explain data. Moreover, there were investigated the fundamental interactions involved when individual single stranded DNA molecules and underlying graphene surface are in contact and when they mutually detach. For that purpose, it was used Single-Molecule Force Spectroscopy (SMFS) with the help Atomic Force Microscope (AFM). Force vs distance curves have been collected inside liquid environment, which show characteristic force plateaus once individual molecules are peeled of from the surface. Plateaus that correspond to desorption of last individual DNA molecule near AFM tip apex are statistically analyzed after experiments, with our data collected into histograms which are fitted with appropriate Gaussian curves. ssDNA chains employed for analysis have been 100 nucleotide long A-homopolymers (adenine), C-homopolymers (cytosine) and T-homopolymers (thymine), forces are measured in temperature range 5 °C - 35 °C, and for different tip velocities of approach and retraction of AFM probe 200 $nm/s - 1500\ nm/s$. Aim of our experiment is to understand the main mechanisms which play a key role in the total interaction between DNA and monolayer graphene surface. Our analysis will show that dominant contributions are hydrophobic and pi stacking interactions, with negligible electrostatic contribution, and we will provide their experimental values. From measurement of dependence of forces on velocity of tip during approach/retraction, we infer that detachment of individual molecules is equilibrium process, which simplifies construction of model to describe experimental data. By studying temperature dependence of total interaction, and developing theoretical model which uses into account contact angle measurements and use of quantity which is called interfacial free energy, we directly connect slopes of experimental fit lines with presence of hydrophobic interactions in the system, while intersects on y-axis give us values of van der Walls force inside the system. As well, exact numerical values of given forces are specified.

1 Introduction

Two-dimensional (2D) materials have recently found an important place in many areas of research, and very important quest in that area is to fully understand properties of given 2D materials in different environments. Comprehension of these materials characteristics can be fruitful in areas such as biophysics, where it is necessary to understand nature of interactions of different biological molecules with these novel materials. In the new millennium, with the coming of the two dimensional materials, the focus of biomolecular detection devices has been shifted towards understanding the physics and the natural biological interactions that these materials manifest. This particular attraction is due to their interesting proprieties and the possibility to exploit them as a new class of biosensor, biomedical devices and single-molecule detection. Nowadays, a substantial effort is provided by research groups in order to discover the models that truthfully explain the behavior behind interactions between biomolecules and 2D materials. The struggle to produce new documentation, experiments and data analysis, will lead to a deep knowledge of this novel field, decreasing the lack of useful information. Following the wave of the study mentioned above and the comprehension of the novel matter, in this thesis experiments and respective analyzes will be exposed regarding the interaction of biomolecules with graphene substrate. To carry out this type of approach, it was necessary to use a specific tool for the scanning probe microscopy (SPM), the *Atomic Force Microscope (AFM).*

1.1 Deoxyribonucleic Acid (DNA)

Since all the experiments in this thesis are made with DNA, we provide a brief description of its properties. In our experiments DNA molecules were used to study their absorption/desorption when interacting with different underlying surfaces. DNA is a biopolymer chain. Polymers are built as a sequence of monomers. Polymer is called homopolymer, when its chain consist entirely of identical monomers, or heteropolymer, when its sequence is build up from different monomer units. Furthermore, biopolymers such as DNA, and some proteins, are also called *polyelectrolytes*. This means that when they are in their natural environments (such as electrolyte solution),

these molecules become positively or negatively charged. In particular,

DNA chain has a largely negative charge due to its chemical composition. Specifically, DNA has a strand structure made up of alternating phosphate groups and deoxyribose rings (sugar). As well, one of the four nitric bases is attached directly to the sugar ring. The nitric bases are: Adenine (A), Cytosine (C), Guanine (G) and Thymine (T). The construct composed of three elements above is called *nucleotide* and it is shown in Fig.1.1(a). There are two types of nitrogen-containing bases, *purines* and *pyrimidines* Fig.1.1(b). Purines consist of a six-membered and a five-membered nitrogen-containing ring, joined together. Adenine and Guanine belong to this class. On the other hand, Cytosine and Thymine are part of pyrimidines, which have only a six-membered nitrogen-containing ring.

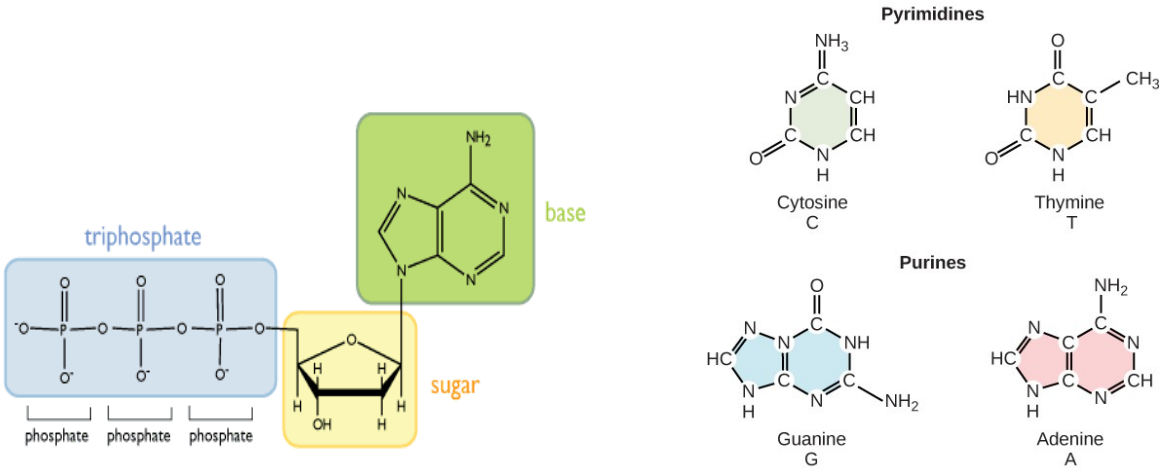

(a) Nucleotide structure **(b)** Nitrogenous bases

Figure 1.1: The image (a) shows the chemical structure of the nucleotide with the triphosphate groups, sugar and the nitric base. The image (b) differentiates the four nitrogenous bases used in the DNA molecules.

DNA molecules in cells typically consist of two sequences of nucleotide strands, which can build the peculiar DNA shape, the *double helix* Fig.1.2. In particular, to build up this structure, is essential that bases in these two nucleotide strands are mutually complementary. For example, if the adenine is in one of the bases in one strand, it will always need to have neighboring thymine in the other strand, and they will form two hydrogen bonds. In the similar manner, guanine must be always coupled with cytosine, and will create three hydrogen bonds. Physically, the reason for this

is that the nitric bases are situated in the core of the double helix, and only pairs A-T and C-G can fit perfectly inside without distorting the double helix structure.[1] As mentioned before, important physical characteristic of the DNA is that its total charge is negative. This charge is provided by phosphate groups. Furthermore, a single helical turn (360) has chain length of 34 Å, the width of the helix is 20 Å, while the distance between each sequence of base-pair is 3.4 Å, as shown in Fig.1.2.

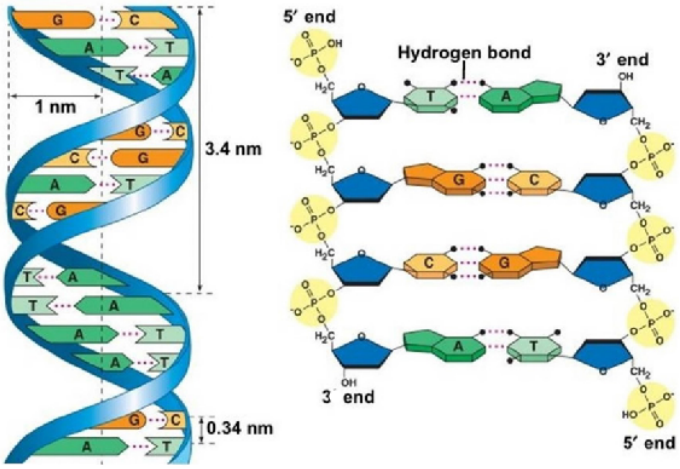

Figure 1.2: On the left side is represented the DNA double helix structure with base pairs distance, helical turn and double strand width. On the right side are shown the single nucleotide sequence strand direction (5'end, 3'end).

1.2 Atomic Force Microscope (AFM)

Atomic Force Microscopy is a technique that derives from the family of Scanning Probe Microscopy (SPM). In this type of class, all the techniques try to replicate the physical surface of the sample, providing a very high resolution output image. For instance, some SPM techniques are: *Atomic Force Microscopy (AFM)*, *Scanning Tunneling Microscopy (STM)*, *Scanning Probe Electrochemistry (SPE)*, *Fluidic Force Microscopy (FluidFM)* and many others. Each of them take advantage from a different setup configuration, based on the various technical specification. In particular, one of the best resolution is given by the AFM. In fact, its resolution is even in order of fraction of nanometers (typically $\sim$ Å in spatial resolution and $\sim pN$ in resolution force). As mentioned, one of advantages of AFM is the ability to image almost any type of surfaces such as ceramics, polymers,

glass and most importantly biological samples. The images are collected via cantilever with a sharp tip which interacts with sample surface, in a raster-scanning mode. When the tip is in contact with the surface, an electrical feedback loop is used to adjust and maintain the height of the cantilever and/or sample supports. This feedback mechanism provides a continuously check during scanning analysis, keeping roughly constant the cantilever deflection. For applications in this thesis, AFM is also interesting because of its ability to analyze several types of tip-surface interactions such as Van Der Waals, electrostatic, mechanical interactions and so on. In particular, in chapter 1.2.3 will be explained in detail the *Force Measurement* involved in this thesis, understanding the relation between force and distance. Typically, in AFM apparatus, a laser beam and a detector are used to monitor the piezoelectric cantilever deflection during the scanning mode, but further detail are provided in chapter 1.2.1.

In this thesis, the focus is mostly put on *AFM based on single-molecule force spectroscopy (SMFS)*, which is a technique used to analyze the molecular forces. In this thesis they have been explored individual molecules mechanical proprieties, in particular, to explore the mechanism behind the interaction and desorption of individual molecules from a specific substrate. In the case of using AFM for single-molecule force spectroscopy, target molecules can be attached either to the force sensor (AFM probe tip), substrate, or both, through chemical or biological manipulation. During our experiments, the molecules will be continuously detached from and attached to the surface of interest, in order to investigate all the relevant molecules proprieties by looking into force vs displacement curves. These curves obtained from several experiments conducted during the thesis period are theoretically explained and analyzed in chapter 3. It is possible to see that many significant and new discoveries related to individual molecules interactions come out from our single-molecule desorption experiments. These help to understand which type of non-covalent interactions, for example electrostatic or hydrophobic, determine the single-molecules absorption/desorption process on the substrate.[2] Furthermore, desorption analysis provides very clear information about absolute force values required to detach individual molecules from surface, which can be useful in other applications, such as biosensing. To conclude, SMFS based on AFM is a well-developed technique which gives access to atomic-scale resolution

and information regarding the interaction of molecules with different substrates, which would not be achievable with other types of SPM techniques.

1.2.1 AFM Working Principles

In general, a AFM is equipped by a silicon or silicon nitride cantilever with a sharp tip which is needed to "feel" or touch the sample surface. There are different types of AFM cantilevers, based on the purpose of the analysis. For instance, AFM cantilevers could be covered with aluminum coating on the back-side to improve laser reflection and have un-coated silicon tip on front for good resolution during imaging. As well, tips and probes can be fully coated with gold to enhance the ease of binding to a biological material, which can be used for analysis of biological molecules. In Electrical Force Microscopy (EFM) a cantilever totally coated with platinum-iridium alloy is used to improve electrical control, to avoid oxidation and charge depletion in doped silicon during experiments. Whereas, in Magnetic Force Microscopy (MFM), cantilevers could be aluminum coated in the back-side while cobalt-chrome alloy coated in the tip side, in order to be properly magnetized before each use with magnetization parallel to the tip axis. Furthermore, there are some cantilever parameters that could be customize (ex. height, width, thickness, half cone angle) based on the specific application. During the approach phase in our force measurements, when the cantilever is brought in proximity of the sample surface, different forces between tip and sample surface will result in a deflection of the cantilever. In order to have a correct physical meaning, this deflection phenomena has to be in the order of nanometers. According with this small deflection, the *Hooke's law* holds:

$$F = -k \cdot \Delta Z \tag{1.1}$$

Deflection of cantilever is modeled as an elastic spring (harmonic oscillator) and the response of AFM probe has opposite of applied external force in equilibrium, hence the negative sign in (1.1). Many material properties can be determined with various AFM techniques, including friction forces, electrical forces, capacitance, magnetic forces, conductivity, viscoelasticity, surface

where F is the external force due to interaction of AFM tip and underlying surface, ΔZ is the small cantilever deflection due to the external force and k is the spring constant. As a result there is a linear relation between deflection and force. Deflection of cantilever is modeled as elastic spring (harmonic oscillator) and the response of AFM probe is opposite of applied external force in equilibrium, hence the negative sign in 1.1. Many material properties can be determined with various AFM techniques, including friction, electrical forces, capacitance, magnetic forces, conductivity, viscoelasticity, surface potential, resistance and many others, as in Fig.1.3 are shown some of these forces.

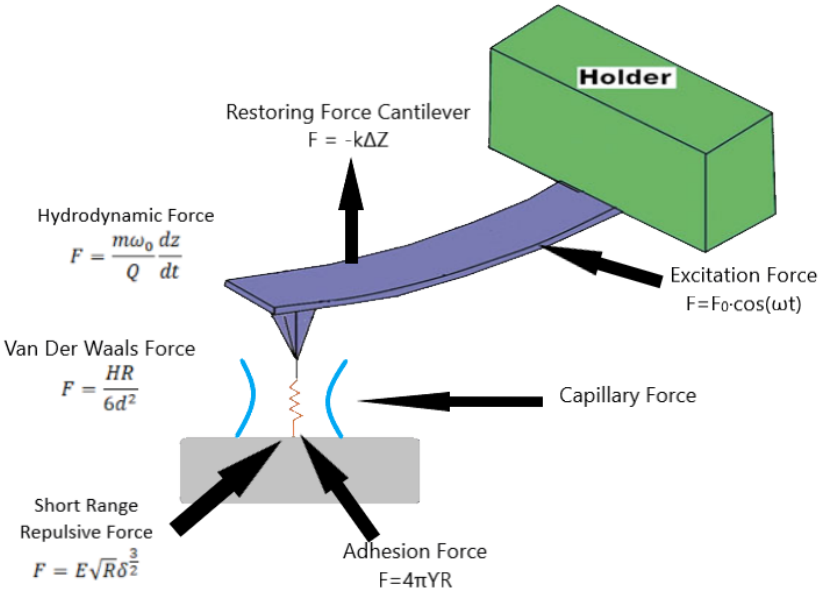

Figure 1.3: In the figure are represented some forces that play a role in the tip-surface interaction. H is the Hamaker constant, E is the Young's modulus, R is the curvature radius of the tip, δ is the indentation depth, k is the spring constant and ΔZ the displacement.

When the AFM probe is sufficiently close to the surface, forces between tip and surface start to be non-negligible, and the cantilever begins to deflect from its initial position. When the interaction between AFM probe and underlying surface is attractive, the tip is attracted towards the sample surface, otherwise the attraction is repulsive and the probe is deflected away from the sample surface. As mentioned above, cantilever deflection is monitored with the help of an optical apparatus composed of laser beam and a very sensitive photo-detector. Typically, laser beam has a well-

defined wavelength and it is pointed directly on the top surface of the cantilever, or backside of the cantilever (usually coated with reflective layer as metal, based on application purpose). The incident laser beam on the cantilever is reflected towards the photo-detector, which collects the laser beam and then transforms the light impulse in an electronic signal. Usually, photo-detector is divided in four quadrants, improving the quality of the deflection detention 1.4. Light can impinge quadrants in 2 modes: normal deflection, where the deflection change the direction on the photo-diode in $\pm$ z axis, and the second mode consists of a lateral deflection, where the deflection leads to a change in $\pm$ y axis. *Positive* and *negative* deflection can be assigned based on where the laser beam interact with the photo-detector. Positive deflection is attributed to the case where cantilever is deflected away form the surface, so laser beam impinges the 2 upper quadrants $V = (V_{III} + V_{IV}) - (V_I + V_{II}) > 0$. On the other hand, when the cantilever is attracted towards the surface, the laser beam hits the 2 lower quadrants, producing a negative deflection $V = (V_{III}+V_{IV})-(V_I+V_{II}) < 0$.

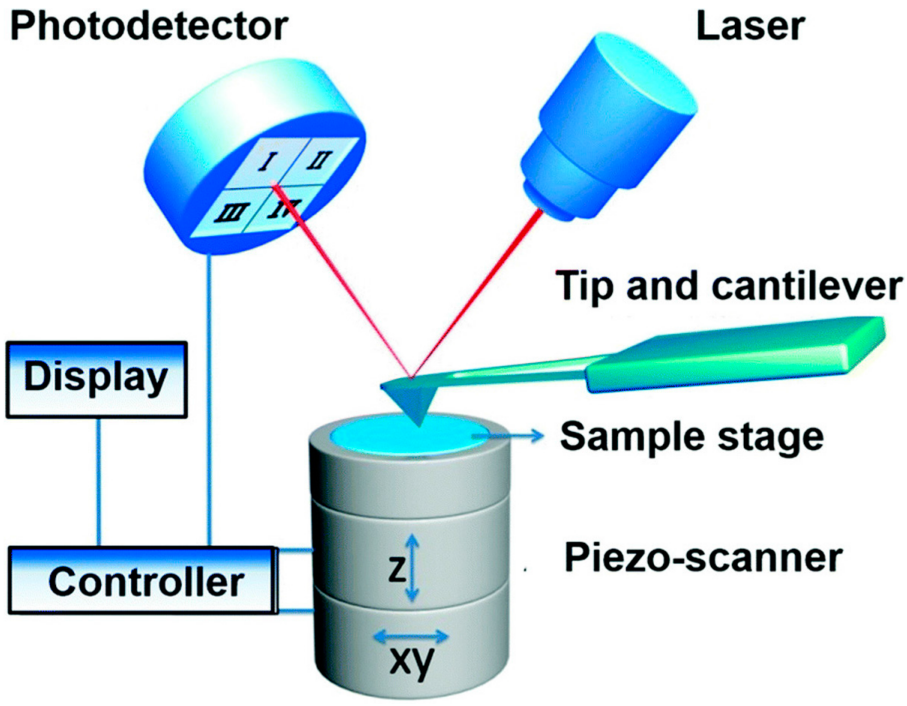

Figure 1.4: In figure is represented the AFM working principle and AFM typical setup [3]

General representation of *Force vs Displacement curve* is shown in Fig.1.2.3. The first stage, when the tip is starting its approach phase,

there is no interaction between tip and surface. As the AFM probe get closer and closer to the surface, external attractive forces appear (Van der Waals, capillary forces) forcing the mechanism *jump into contact* of the tip towards the surface. In this second stage, the AFM probe snaps-in towards the surface causing a cantilever deflection towards the specimen. Any further approach after jump into contact will result in more positive deflection which will bring the cantilever in a position with zero deflection and direct contact with sample surface. In the third stage, when contact is established, force is positive and the cantilever is deflected away from the surface, to our loading force value. Then, a retraction step can begin. Since the tip is firmly pressed on the surface, in retraction region must be taken into account the attractive adhesion force. Contrarily to approach stage, step four again brings cantilever deflection to zero changing deflection from positive to negative. During the fifth stage, AFM probe is attracted to the surface because of attractive adhesion forces and cantilever deflection is negative. In this stage, adhesion force continuously increase its negative value until it reaches a maximum negative value during any further retraction. At this point, AFM tip abruptly jumps off from the surface, bringing cantilever deflection to initial zero value, shown in phase six. From now on the tip and sample are no longer in contact and they do not interact. The curve in Fig.1.2.3 is a general force vs displacement curve obtained by force spectroscopy analysis. Tip/surface modification with biological materials can provide a slightly different shape and features on collected experimental force vs distance curves. This change of look has to take into account some other external factor such as noise (thermal, electrical, mechanical etc) and other possible source of contamination in measurement that might be affected the final appearance of force/distance curves.

As mentioned in the previous chapter, AFM has abilities to make a surface image. AFM imaging modes can be divided in *static (or contact) modes* or *dynamic (tapping or non-contact) modes*. A brief description of these modes is developed below, with the awareness that during the thesis, the experiments were carried out in contact mode, to which more focus on it will be given in subsequent chapters.

Contact Mode

This is most common mode used when working with AFM. In imaging, the tip is brought into contact with the sample surface, allowing it to be scanned in x-y direction. During the surface navigation, the tip is kept at a constant height with the help of a continuous check on the cantilever deflection. The deflection of the cantilever is adjusted through a feedback loop which move the cantilever or sample stage up or down according to the desired set height value or deflection value. This precise movement is possible due to the voltage applied to very sensitive piezoelectric material which raise or lower the tip/sample position, restoring the deflection value chosen as a native parameter in AFM system. Typically, when the tip is approaching the surface, the attractive force plays a fundamental role, producing a phenomena called "snap-in" or jump into contact. This means that the tip, literally, jump into contact with the surface at a certain gap between them. The contact mode force analysis starts to be performed when overall force is repulsive, so the tip/surface are in close contact with each other. On the other hand, when the tip is retracting from the surface, adhesion attractive forces dominate. In fact, to have the total tip retraction, the adhesion force has to be lower than the lever traction, so the cantilever can jump off contact from the surface. This mechanism is completely explained in Fig.1.5 with a typical force vs displacement curve in contact mode. The contact mode procedure can be implemented by immersion of the sample and tip in liquid. With this approach, there are many advantages that can help to analyze the influence of sample environment or avoiding forces which complicate the comprehension of tip/sample interaction. For example, in liquid there is a complete removal of capillary forces and a substantial reduction of Van der Waals' forces. Furthermore, working in immersion can help to determine relevant force contributions to total interaction, and to understand the processes happening at liquid/-solid interfaces.[4]

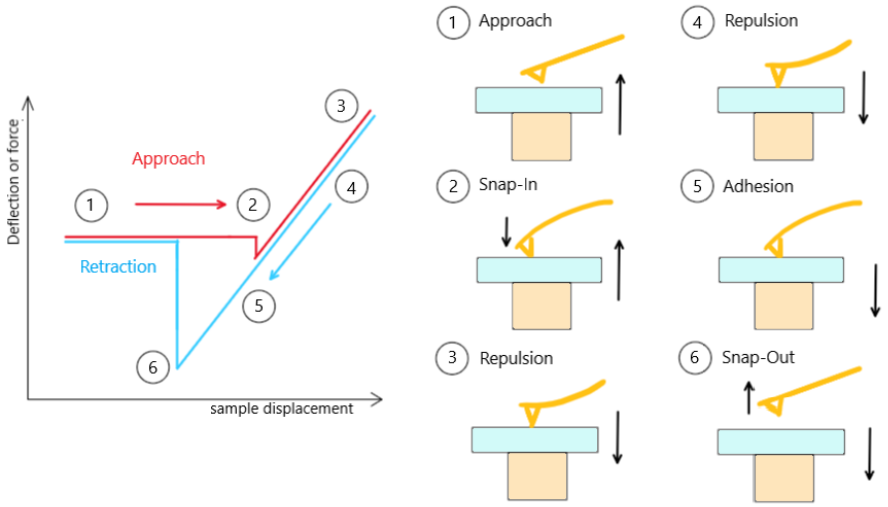

Figure 1.5: Schematic representation of the principles attraction-retraction force in AFM contact mode. In the second step is visible how the tip is attracted on the surface, while in the sixth step the tip jump off contact form surface.[5]

Since tip is in hard contact with surface during experiments, the stiffness of the cantilever has to be less than the effective spring constant which keep atoms together. This range is around $1 \sim 10\ nN/nm$. The major problem in contact mode is that some samples develop a liquid meniscus layer during the measurements, which can be a problem from measurement that are not in liquid environment, and in that case the use of inert gases is a must. For this reason, in ambient conditions, a dynamic mode analysis is preferable.

Tapping Mode

Tapping mode is the most commonly used mode within the family of AFM dynamic modes. Its working principle consist of guide the oscillation of the cantilever up and down near its resonance frequency on the underlying surface. This swing mechanism is achieved with the help of a piece of piezoelectric material placed in the cantilever holder. An electronic feedback is needed to keep constant the cantilever oscillation and to check either the amplitude or the phase of this frenetic movement. Typically, the amplitude of this oscillation wanders around few nm up to 200 nm. For imaging, tapping mode has a higher resolution compared to contact mode.

This increase in resolution is a result of avoiding the tip-surface drift and absence of lateral movement, since tip is barely in contact with surface, compared to static mode. In detail, the image is produced by evaluating the force of the intermittent contacts between tip and sample. With this mode is possible to scan larger part of the sample, for instance 20 nm, or go to get more smaller details of surface reducing the scanning area to 5 nm. Further example are shown in chapter 2.3.3. When the tip is approaching the sample in tapping mode, forces such as Van der Waals, dipole-dipole interactions or electrostatic interactions can affect the amplitude oscillations. The feedback loop adjust the z-position of the tip during the scan process which gives us surface topography,[6] as show in Fig1.6. Since the tapping duration on the surface is relatively short, the peak force applied during the scanning can be higher than the force used in contact mode. However, this greater applied force does not drastically damage neither the tip nor the underlying surface, as happens during the static mode.

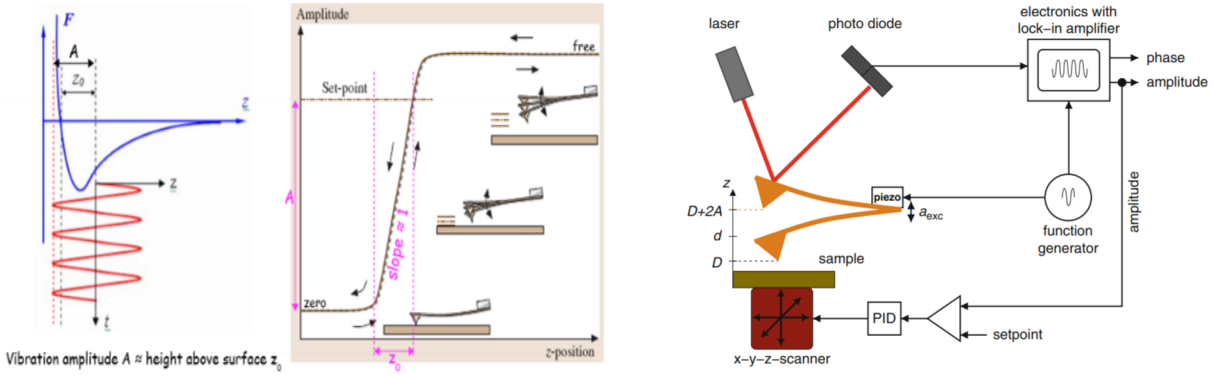

(a) Tapping Mode Force vs Displacement

(b) Tapping Mode Setup

Figure 1.6: Schematic representation of the principles attraction-retraction force in AFM tapping mode (a). Schematic setup (b) with Lock-in-Amplifier which regulate the feedback signal to keep amplitude constant.[6]

Non-Contact Mode

Regarding AFM in non-contact mode, the tip never interact directly with the sample nor touches the surface, contrary to what happens in tapping or contact modes. This means that the tip is always kept at a certain distance from the top of the sample surface, without touching

the surface Fig.1.7. To maintain this gap, the cantilever is rocked to its resonant frequency (frequency modulation) or a bit over, called amplitude modulation, where the amplitude oscillation has a range from less than 10 *nm* up to picometers quantities, as mentioned in *Leo Gross, et al.* work.[7] When the tip approaches the surface, without touching it, tip movement is affected by attractive Van der Waals forces in which this interaction causes a change in both the amplitude and phase of the cantilever oscillation. The swing alteration of amplitude and frequency is monitored by a *z-servo system* feedback loop, which transforms the mechanical tip motion in a electrical signal in which this signal commands the motive apparatus of the tool in a predefined set point. In the end, a modification in cantilever oscillation triggers a feedback signal which adjusts the cantilever position during the surface scanning. This sequence of events allows to construct a topography image of the underlying sample. Typically, nc-AFM is more suitable for soft specimens, than other techniques, because it does not stick on the surface and thanks to this fact, both tip and sample do not suffer from degradation but resolution might be significantly lower compared to tapping mode.

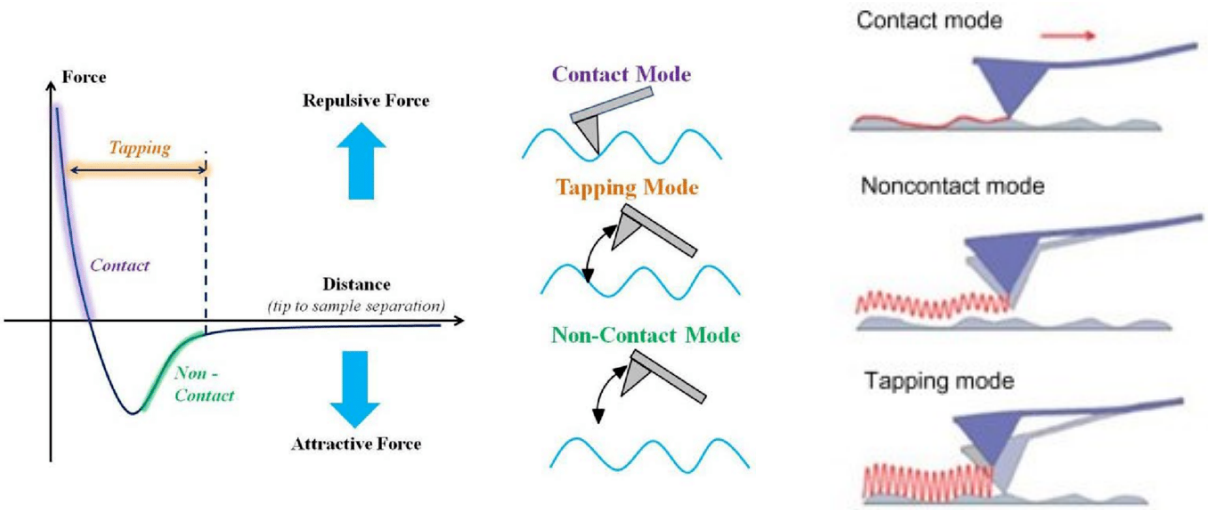

(a) Force vs distance curve of the 3 AFM approaches

(b) Working principal of the 3 approaches

Figure 1.7: Figure (a) represents the force applied versus the tip-sample distance. The contact mode operates in the region close to the surface where the Coulomb forces are highly repulsive. The non-contact mode operates far from the sample and is sensitive to the attractive Van der Waals forces. The tapping mode oscillates between contact region and non-contact region.[8] In figure (b) are represented the 3 imaging scanning modalities: contact, non-contact and tapping modes[9]

1.2.2 Calibration of AFM tips for SMFS experiments

In chapter 1.2.1 was mentioned which parameters are important when someone is dealing with AFM tool. In particular, with the help of Hooke's equation 1.1, it is possible to extrapolate 3 important values: AFM probe spring constant, cantilever deflection and external force. By knowing the spring constant of AFM cantilever and *nm* cantilever deflection in z direction from our measurements, it is possible to determined the interaction between tip and sample surface. In this thesis, *AFM Cypher ES* microscope provided by *Asylum Research* was used for experiments. With this powerful tool, 2 important parameters will be extrapolated and explained from measurements. They are: *spring constant (k)* and *inverse optical lever sensitivity (InvOLS).*

For what concerns tip calibration, this AFM provides a precise software tool to determine efficiently the spring constant. The tool is called GetReal^{TM} and it is briefly present in this chapter. First of all, when Asylum software is initialized, in order to calibrate the tip, it is needed to examine the thermal noise spectrum provided by the AFM tip. This spectra take into account the large range of frequencies, trying to avoiding external noises on the tip in air environment (tip calibration is done either before or after the experiments in air environment). Logically, the graph in Fig.1.8 has different peaks with several details concerning technical noises and environment noises. Our peak of interest is the one between the red line confinement and it represents Lorentz's shaped peak. This means that the AFM tip is oscillating at or near its basic resonant frequency in air. So this peak depicts fundamental tip oscillation mode and it is easy to visualize it in the thermal noise spectrum, since it has largest amplitude in power density spectrum.

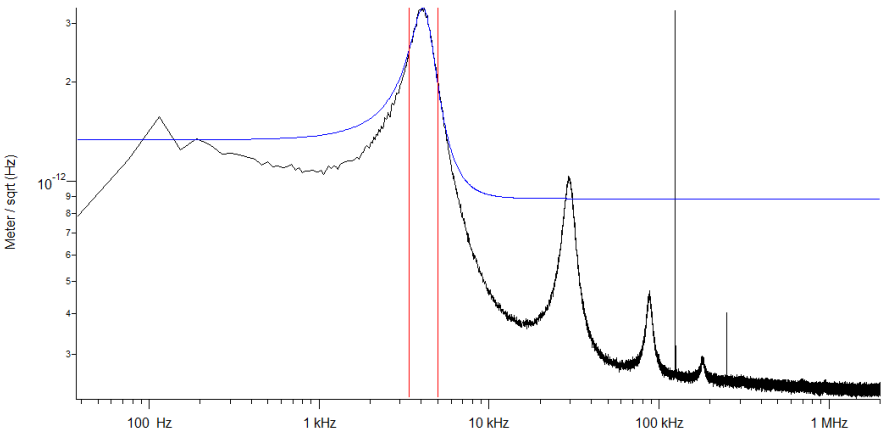

Figure 1.8: Spectral power density used to calibrate AFM gold tip.

During tip calibration, it is possible to choose which method is the most suitable for the current tip calibration or which technique AFM tool provides to automatically calibrate the tip. In this Asylum AFM, *Oxford Instrument Group* selects the Sader's method to gauge the tip. This method simplifies the calibration of the tip to determination of spring constant to the one of mechanical harmonic oscillator. Furthermore, Sader's method enables to determine and view the spring constant considering only the plan view dimensions of the cantilever (length and width), its fundamental resonant frequency and quality factor in air.[10] These previous attributes are usually written on AFM probes box, except for the quality factor. The latter has to be determined through power density spectra and unless malfunctions or anomalies are present, this parameter is determined in the Lorentz's peak fit inside range shown in Fig.1.8. Since during the development of this thesis was used a rectangular cantilever, in the beginning the spring constant could be defined considering the following equation provided by Sader et al.

$$k = M_e \rho_c t w L f^2 \tag{1.2}$$

where f is the resonant frequency, t, w and L are thickness, width and length, respectively. ρ_c is the density of the cantilever and M_e is the normalized effective mass. Nevertheless, this formula provides some limitation regarding the effective mass and cantilever thickness and does not provide any dependence about quality factor in air. For this reason, after some

mathematical rearrangements, Sader et al.[10] give a straightforward equation to determine the AFM probe spring constant

$$k = AQwLf^2 \tag{1.3}$$

where f, w and L as before are resonant frequency, width and length, respectively. Q is oscillation quality factor in air and A is numerical constant provided by Sader et al.

When spring constant is determined, the second important parameter to take into account is inverse optical lever sensitivity (InvOLS). During a cantilever deflection, the signal coming out by photo-detector is in Volts, so there is a necessity to convert this Volts signal into more physical nanometer units, and this conversion is provided by InvOLS. In fact, InvOLS unit is a ratio between displacement of cantilever in nm per voltage unit (nm/V). As in the case of the quality factor Q, InvOLS is determined through the analysis supplied by thermal power density spectra, where the resonant Lorentzian's peak is fitted by the following equation

$$P(f) = P_{white} + \frac{P_{DC} f_R^4}{(f - f_R)^2 + \frac{f^2 f_R^2}{Q^2}} \tag{1.4}$$

where f is frequency, f_R is resonant frequency, P_{DC} is magnitude of spectral power density for cantilever oscillation (V^2/Hz) measured by photo-detector, Q is oscillation quality factor in air and P_{white} is spectral noise density of white noise (V^2/Hz). With the help of the *Asylum's* software tool, thermal power density spectra is determined and resonant peak of fundamental mode is fitted with the equation 1.4, and parameters as Q and P_{DC} are obtained. Integrating equation 1.4 over all oscillation mode frequencies, it is clearly possible to understand how the mean square voltage fluctuations $\langle \Delta V^2 \rangle$ are expressed as a function of Q and P_{DC}. Since the definition of InvOLS consist of a ratio between RMS (root mean square) cantilever fluctuations over RMS voltage fluctuations, the relation becomes:

$$\langle \Delta z^2 \rangle = \frac{\pi}{2} InvOLS^2 P_{DC} Q \tag{1.5}$$

Furthermore, when the partition theorem is taken into account, cantilever fluctuations is seen as thermal fluctuation:

$$\frac{1}{2}k\langle\Delta z^2\rangle = \frac{1}{2}k_B T \tag{1.6}$$

where k_B is the Boltzmann constant and T is absolute temperature. All the term on the right side of equation 1.6 represents the average thermal energy for each degree of freedom, where degree of freedom means all the possible energy modes.

Combining equation 1.5 with 1.6 the InvOLS value is easily accessible knowing the real value of spring constant k:

$$InvOLS = \sqrt{\frac{2k_B T}{\pi k Q f_R P_{DC}}} \tag{1.7}$$

In general, calibration could be carried out in two different main environment: air or liquid. For the purpose of this thesis project, each AFM probe calibration was performed in air condition, where error is lower compared to liquid environment. In particular, when measurements of forces between DNA and sample were over, every liquid contaminants were eliminated with high purity ethanol and dried with nitrogen in order to allow spring constant calibration. The cantilevers supplier writes the nominal value of spring constant in air on the box. Having this nominal value and changing it (in Asylum's software) will give a InvOLS numerical value adjusted to the real measured spring constant value. The real spring constant value is obtained taking into account noise power spectra on 10 different laser beam positions on AFM cantilever in air. Furthermore, from measurements on these 10 positions we obtain mean spring constant value by applying statistical formula over all measured the spring constant values.

$$\mu = \frac{\sum_{i=1}^{N} x_i}{N} \tag{1.8}$$

where μ represents the spring constant mean. Moreover, standard deviation helps to obtain a real value of spring constant considering the calibration error. In the case of this thesis, the error is more less than 5%.

$$\sigma = \sqrt{\frac{\sum_{i=1}^{N}(x_i - \mu)^2}{N}} \tag{1.9}$$

in which σ represents the standard deviation of the spring constant mean. Combining equation 1.8 and 1.9 is possible to obtain the real value of the spring constant under analysis:

$$k_{real} = \frac{\sum_{i=1}^{N} x_i}{N} \pm \sqrt{\frac{\sum_{i=1}^{N}(x_i - \mu)^2}{N}} = \mu \pm \sigma \tag{1.10}$$

where the first term is the average formula, second term indicates standard deviation formula, while N corresponds on the 10 different positions of the laser beam on the cantilever surface, and μ points out the spring constant mean value.

1.2.3 AFM Force vs Distance Curves

In addition to being a fascinating tool for topographical analysis, AFM is also a tool that allows much more specific analysis of interactions between tip and surface through the study of the *Force vs Distance* curves. There are many reason why they are collected and analyzed. These curves can be sometimes used to measure for example the viscoelastic propriety of a certain material or even its stiffness. When individual molecules are involved in force-distance analysis the method is known as *"Single-Molecule Force Spectroscopy (SMFS)"*. Often in this thesis, force spectroscopy will be related to analysis of interaction between biological molecules and 2D material. However, force-distance curves of biological molecules interacting with underlying sample surface can have some common elements with non-biological curves, but there is a substantial difference regarding observed features during detachment (retraction) of individual molecules in force spectroscopy. In particular, force-distance curves obtained from individual molecules display a large adhesion peak negative force during first stage of retraction in Fig.1.9. After this stage, there are noticeble new features, different number of abrupt force jumps, depending on how many molecules are positioned on the top of the AFM tip, and are detached/peeled from underlying substrate with a constant force for each individual DNA molecule. Furthermore, from our measurements, as it will be seen in thesis (confirming previous observations from Suresh Manohar et al.[11]), peeling of molecules is a steady state process (constant force). All further informa-

tion on analysis of force jumps and their meaning will be expressed in Chapter 2.3.2 and Chapter 3.1, respectively.

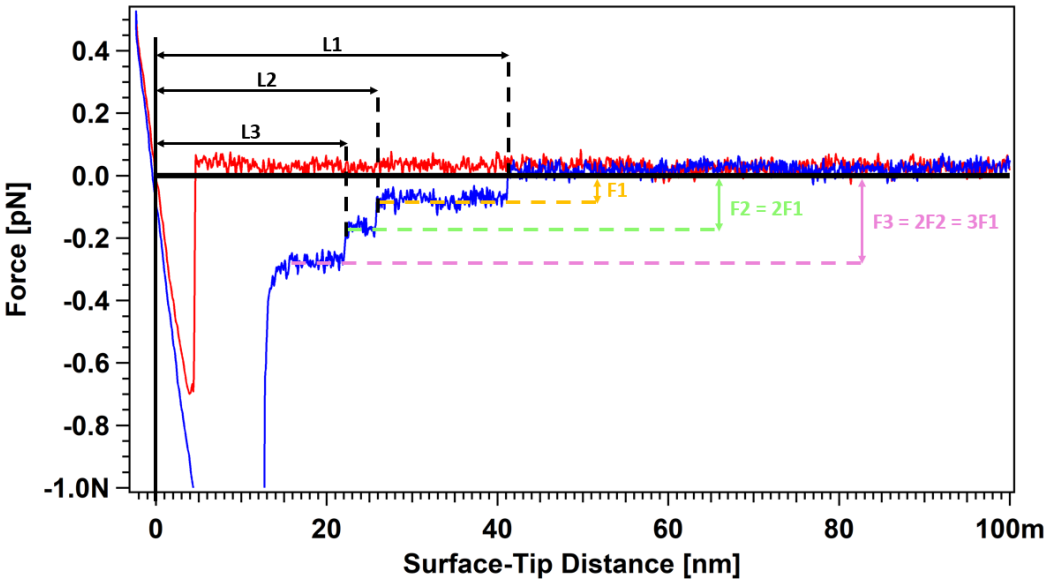

Figure 1.9: The graph represents the approach-retraction process with multiple DNA peeling steps. The complete molecules peeling produces an abrupt jump during retraction.

Our force spectroscopy curves are not characterized only by force jump numerical values, but also with plateau length during measurements. This means that force jump value of last step or its plateau lenth, have to match a range of values to be considered as a real, meaningful DNA peeling event, as it is shown for last peeling step in Fig.1.10(a). To the best of my knowledge, during the experiments with A-homopolymers, C-homopolymers and T-homopolymers, their force jump had to remain in the range between $30 - 100\ pN$, otherwise force jump value might be affected with contaminants inside liquid environment or contaminants on sample surface. When force range is within our specified limits, it was also a must to check the plateau length, which can have a maximum equal to the nucleotide chain length. ssDNA oligomers used in our experiments were composed of 100 nucleotides ($6.76\ \text{Å} = 0.676\ nm$ per each nucleotide length[12]), which means that maximum length of this final step is up to $70\ nm$. Moreover, there is a chance where the constant peeling of DNA molecules does not succeed when a unstable force event happens. This change in force produce a change in force-distance curve, distorting the plateau. In fact, in Fig.1.10(d) just

before the jump, DNA molecules have a different peeling force in the beginning of the step compared to the end of the step, due to a non-uniform conformation of the underlying substrate, producing a parabolic bend in the plateau just before the complete tip retraction.

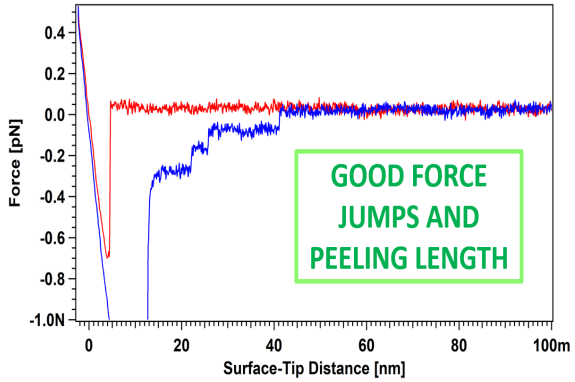

(a) Curve to take into account during the analysis

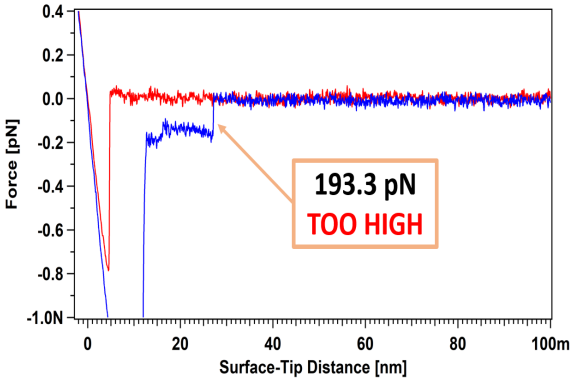

(b) Force jump too high

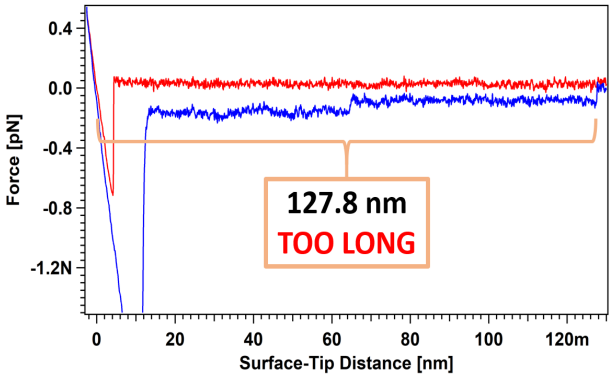

(c) Molecules peeling distance too long

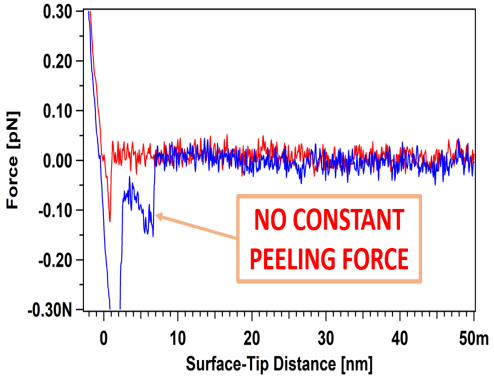

(d) of a DNA molecule due to the higher force

Figure 1.10: The images (a), (b), (c) and (d) represent four different force vs distance curves during a ssDNA molecule desorption from monolayer graphene on SiO_2/Si surface. In (a) is shown an analysable curve composed of three peeled molecules with the correct force jump values of last molecule peeling. The graph on the top right corner (b) points out a peeling force that is too large while (c) indicates a step that is too long due to some contaminates. Chart (d) is displays the different force pattern where the constant peeling behavior is distorted due to noise and this curves are not analyzed.

1.3 Graphene and Materials Proprieties

In this chapter there will be explained some general proprieties of materials relevant for this thesis project. Particular focus is put on Graphene and Graphite, while other type of 2D materials as hexagonal Boron Nitride (h-BN) and Molibdenum Disulfite (MoS_2) could not be analyzed

for the thesis' purpose because of the unpleasant experience and lockdown due to the COVID-19. Referring to 2D materials, usually means crystalline materials with single layer of atoms, packed or organized in a lattice structure. In the case of *Graphene*, its structure consist of a single-layer composed by carbon (C) atoms organized in a hexagonal lattice Fig.1.11. This pattern, such a honeycomb structure, forms a single graphene sheet. Each C-atom is covalently linked with the three neighboring atoms, forming one σ bond with each of the three neighboring atoms and one π bond. Due to its covalent bonds, graphene shows a great stability and high tensile strength. The distance between each neighboring atom is about 1.42 Å (0.142 nm). Graphene can be found in different physical shapes such as powders, flakes, ribbons, and sheets and others.[13] Moreover, graphene is a zero-gap semiconductor, which means that it behaves as a metallic material when the difference between conduction and valence band (bandgap) is zero, or it acts as a semiconductor when the gap is different from zero. This double behavior is usually seen in graphene nanoribbon (GNR), where the sheet width size is less than 50 nm, and based on the direction it is possible to choose two pattern: zig-zag and armchair.[14] The first presents pure metallic behavior, while armchair shows a metallic behavior with small GNR size and a bandgap different from zero when GNR size increases. Furthermore, graphene shows good performance in terms of electron transport. As a matter of fact, it presents a very high electron mobility about 200000 $cm^2V^{-1}s^{-1}$ at a carrier density of 10^{12} cm^{-2} which is million times greater than copper mobility.[15,16,17] Also at room temperature, electrons in graphene can present ballistic behavior, which means they can travel without collision/scattering up to micrometer distances.[18] Besides, graphene exhibits an extraordinary thermal conductivity in the range of $\sim 3000 - 5200$ $Wm^{-1}K^{-1}$.[19] In terms of mechanical proprieties, graphene is the strongest material discovered up to now even stronger than diamond.[20,21] The reason for that lies in the fact that graphene atoms are tightly bonded providing high stability and strength. Its tensile strength is about 130 GPa while its stiffness (Young's modulus) is about 1 TPa. Another peculiarity of graphene is tunability through plasma and chemical engineering techniques, making it the most used material concerning biosensing and single molecule detection application.[22]

When several graphene sheets are stacked on top of each other, the

structure is called multi-layer graphene, while very thick stack of 2D material makes *Graphite*. As well as graphene, graphite is a crystalline form composed by C-atoms rearranged in a hexagonal shape Fig.1.11. This material is the most stable form of carbon in standard condition as room temperature and room pressure. Typically, around more than 30 graphene sheets build up a graphite bulk. Graphite is a bulk material in which graphene sheets are interacting via weak van der Waals forces allowing easy separation of layers. The distance among graphene planes is 3.35 Å (0.335 nm). Its density varies in range 2.09–2.23 gcm^{-3}. Compared to diamond, it is less dense because of a gaps between layers. Moreover, because of its delocalized electron are moving as well between planes, graphite can conduct electricity making it useful for application such solar panels, electrodes, electrochemistry and others. As well it could be transformed into diamond when high pressure and temperature are applied. Furthermore, graphite is used in single molecule force spectroscopy making it suitable for the purpose of analysis in this thesis.

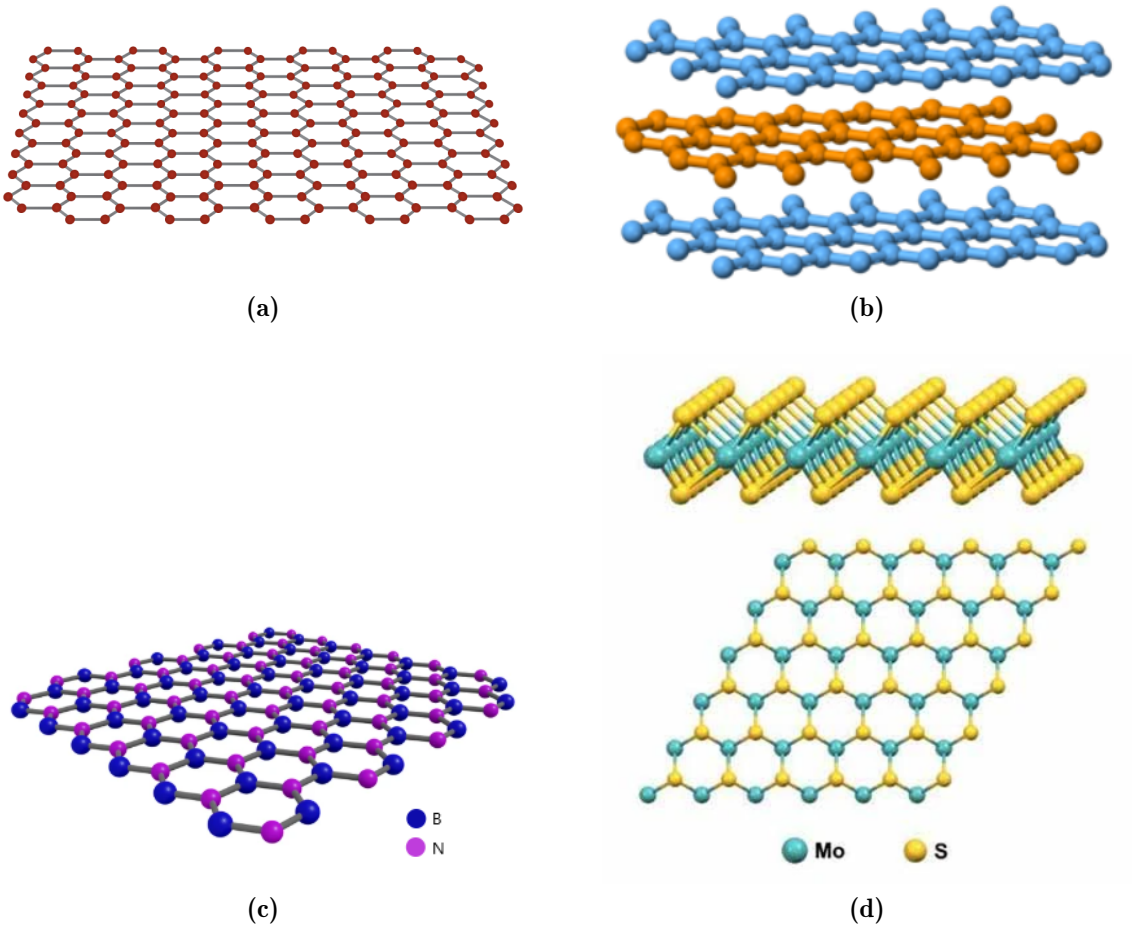

Figure 1.11: The four figures represent the atomic structure of the materials used during the SMFS experiments (a) graphene and (b) graphite and the materials that there will be analyzed in future experiments (c) h-BN and (d) MoS_2.

In the set of materials that should have been studied during this thesis project it should be mentioned *hexagonal Boron Nitride (h-BN)*. This is a two-dimensional material composed by boron (B) and nitrogen (N) atoms in which they alternate their atom sequence arrangement Fig.1.11. These arrangement could be made in different structures such as hexagonal (h-BN, similar to graphene), planar, cubic (c-BN, similar to diamond) and wurtzite. The B-N atoms in monolayer h-BN are arranged to have a distance of 1.45 Å between neighboring atoms. The bond between B-N is a strong σ bond, providing a very stable covalent bond between the different atoms. Adjacent layers of h-BN sheets in bulk interactvia weak van der Waals bond, with an interlayer spacing around 3.33 Å (0.333 nm), bit less compared to graphene's interlayer. The existence of in-plane and local

dipole moments inside the lattice due to the convalent B-N bond, makes this material very interesting in term of proprieties. Monolayer h-BN is an insulator with large bandgap ($\sim 5.9\ eV$). Besides that, h-BN shows other important proprieties. It can not decompose up to a temperature over 1000 °C in air and 1400 °C in vacuum, thermal conductivity is similar to the graphene ($\sim 1700 - 2000\ Wm^{-1}K^{-1}$), placing it as one of the best thermally conductive materials. Coefficient of thermal expansion is around $-2.90 \cdot 10^{-6}\ K^{-1}$, and bulk modulus is 36 GPa.[23] These proprieties make this material affable for the biosensory market as mentioned in Liuyang Zhang and Xianqiao Wang paper in which they explain how to provide a DNA sequencing with hexagonal boron nitride nanopore.[24]

Another 2D material to take into account in possible experiments is *Molybdenum Disulfide (MoS_2)*. Its crystal structure is made by a sandwich between the 2 S and one Mo atoms. This crystal structure forms a hexagonal plane of sulfur atoms on both sides of a hexagonal plane of molybdenum atoms. This 3 layers structure packed on top of each other is kept compact with the help of strong covalent bonds between Mo-S atoms, while layers in bulk are held together with weak vand der Waals forces. The distance between Mo-S atoms is 2.39 Å, with an interlayer distance around 6.5 Å. The bandgap for this kind of material is similar to silicon, and it shows an indirect bandgap of $\sim 1.2\ eV$.[25] In accordance with this thesis, MoS_2 is also used in the study of single molecule detection.[26]

2 Experimental Setup and Materials

In this chapter, sample preparation procedures and experimental methods used for characterization of materials are explained such as Raman spectroscopy and AFM imaging in tapping mode. Material preparation techniques in cleanroom, and chemical laboratories are explained, together with procedures that are required to clean samples from contaminants.

2.1 Preparation of Au-coated AFM Tip

2.1.1 Materials

The basics material were purchased from Singapore and Belgium. In particular, Au-coated AFM tips come from Crest Technology Pte Ltd (Singapore) and gold tip model is ContGB-G Budget Sensors. Nuclease-free HyClone HyPure Molecular Biology-Grade water was the deionized water useful in all experiments where DNA molecules were used and it was purchased from GE Life Sciences (Singapore) and stored in fridge at 4 °C. Salts were bought from Sigma-Aldrich (Singapore) and 2 of them, Sodium phosphate monobasic (ReagentPlus grade) and sodium phosphate dibasic (BioReagent grade), were used to prepare the buffer solution for measurements, while sodium chloride (BioXtra grade) was needed during tip functionalization process. To clean surfaces and tools was used Ethanol (HPLC grade), purchased from Merck (Singapore). Dried form of disulfide-protected thiol modiefied DNA oligomers (PAGE purified) was adopted to protect DNA molecules from degradation and it comes from Eurogentec (Belgium). ssDNA moelecules were dissolved in 10 mM phosphate buffer and stored at $-20\,^{\circ}\mathrm{C}$ before use. Three different DNA chains were employed during experiments, one was ssDNA A-homopolymer or polyadenine with 100 nucleotides (nt) long ($5' - A_{100} - Spacer18 - Spacer18 - O - (CH_2)_3 - S - S - (CH_2)_2 - OH - 3'$), the second sequence consisted of ssDNA C-homopolymer or polycytosine long 100 nt ($5' - C_{100} - Spacer18 - Spacer18 - O - (CH_2)_3 - S - S - (CH_2)_2 - OH - 3'$) while the third chain was composed by T-homopolymer or polythymine with 100 nucleotides (nt) long ($5' - T_{100} - Spacer18 - Spacer18 - O - (CH_2)_3 - S - S - (CH_2)_2 - OH - 3'$). From Sigma-Aldrich (Singapore) 6-mercaptohexanoic acid 90% ($C_6H_{12}O_2S$) and Tris (2-carboxyethyl) phosphine hydrochloride solution were purchased and stored at $-20\,^{\circ}\mathrm{C}$ and in nitrogen dry box, respectively.

2.1.2 Functionalization and modification of AFM gold tips with DNA oligomers

Since biological material were employed in this process, all the material handling were performed with maximum attention to cleanliness and un-

necessary contaminations in solution or expwrimental setup were avoided at all times. In literature, functionalization of AFM gold-coated tip with DNA[27] is well described, and functionalization in this thesis is pretty similar, with some slight modifications. First of all, gold tips were cleaned of contaminants in plasma machine (CUTE, Femto Science, Korea) by using H_2 plasma, which is less aggressive, compared to O_2 plasma. The latter could oxidize the surface of the gold tips and prevent binding of thiol group of DNA onto gold coated tip. This cleaning step also enhances the probability of successful modification of the tips and success rate of the experiment.[28] To perform the cleaning process, the following parameters have been framed: H_2 plasma power of 15 W, H_2 gas flow of 15 $standardcubiccentimetersperminute(sccm)$ for a period of time of 60 s. Once plasma step is finished, Au tips have to be deposited to the bottom of a 1 mL glass container with DNA solution for further steps. In the meantime, separately, DNA solutions are prepared. In detail, freshly 10 mM phosphate buffer solution with 2 different $NaCl$ salt concentration are used. 1 M was used to functionalize tips and 0.1 M was used to store tips at 4 °C in fridge, in case tips were not immediately used in experiments. Salt weight needed to prepare solutions was obtained via manipulating the following equation:

$$C = \frac{m}{M \cdot V} \tag{2.1}$$

where C is the solution concentration, m is the mass quantity to calculate, M is the molecular weight of salt and V is the phosphate buffer volume. Buffer solution with 1 M NaCl added salt is needed for modification in order to prevent electrostatic repulsion between individual DNA molecules during gold tips modification.[29] Prior to DNA solution preparation, stock DNA was pulled out from freezer at -20 °C and left to warm up for $25-30$ minutes in order to resuspend DNA molecules. Then, for DNA dilution in phosphate buffer to required modification concentration, it was used an initial stock DNA concentration of 100 μM and reached final concentration of 0.3 nM 2.1. Dilution steps where performed with the help of *dilution equation*:

$$C_i \cdot V_i = C_f \cdot V_f \tag{2.2}$$

where C and V are concentration and volume, respectively, while the subscript i and f point out the initial and final, respectively.

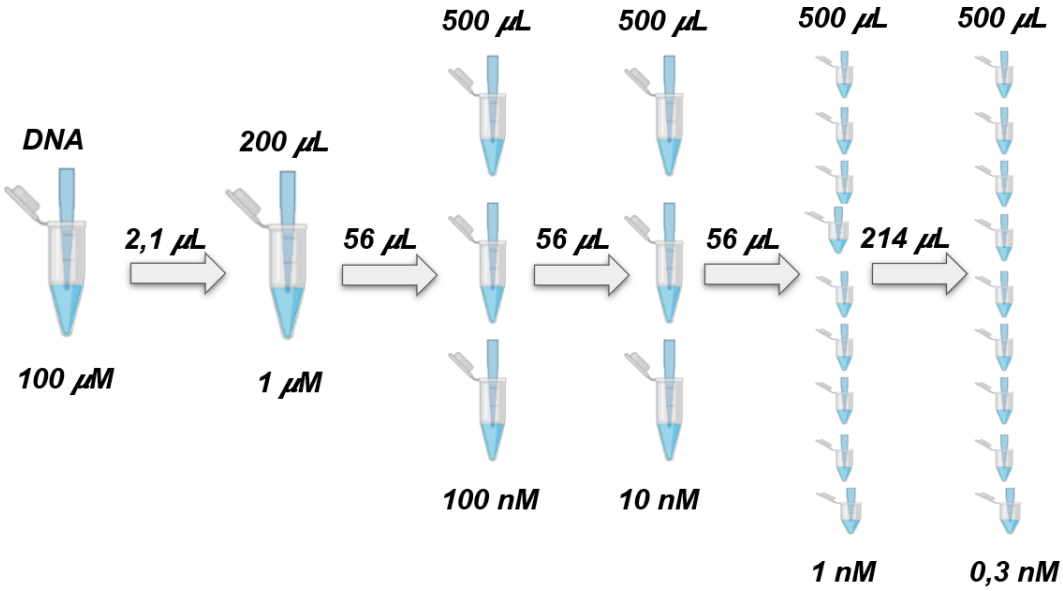

Figure 2.1: Representation of the dilution steps, from the DNA stage up to the final solution having a concentration of 0.3 nM.

Immediately after dilution process, 12 μL of 10 mM *tris2-carboxyethylphosphine* (TCEP) solution was added into final DNA in buffer (0.3 nM) solution, and left to react for one hour while covered with aluminum foil because of the photosensitive nature of TCEP. TCEP is a reducing agent which allows breaking of disulfite bonds at thiol termination of DNA molecules, permitting a direct covalent link between thiol groups and gold tip.[29] Once Au tip is immersed in our complex solution (buffer, salt, DNA and TCEP), it has to rest for one hour in order to allow the DNA-tip covalent attachment to take place. Then DNA-tip is hydrated with HyPure water and rinsed with HPLC ethanol and immersed again into a solution composed of 1 mL of HPLC ethanol and 2 μL of 12 mM *6-mercaptohexanoic* acid (6-MHA) solution for 1 hour.[30] 6-MHA acts as a spacer preventing unnecessary DNA sticking to Au surface 2.3.

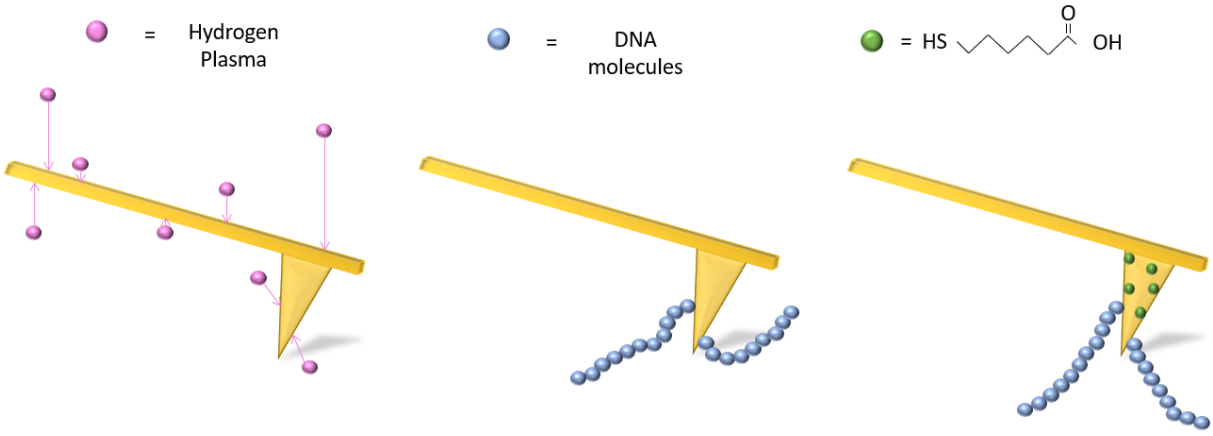

Figure 2.2: The figure represents the 3 processes involved in order to obtain a tip ready to be analyzed. On the left is shown the hydrogen plasma process, in the middle is point out the bond between DNA molecules and gold tip with a particular focus on the DNA folding towards the tip, while on the left side is shown the final stage of the entire tip preparation process in which the 6-MHA prevent the folding and sticking of DNA molecules on the Au-probe.

6-MHA has the carboxyl ($-COOH$) termination on one side of alkane chain and thiol ($-HS$) termination on the opposite side.[30,31] Besides, these SAM molecules are successful to prevent DNA sticking, and help us in directing DNA molecules directly into the liquid environment and towards the underlying material surface, because they provide an additional electrostatic repulsion to phostphate backbone of DNA. Moreover 6-MHA prevents nonspecific interaction between Au tip and analyzed substrate.[27] After the right amount of time to favor the reaction, last rinsing step was performed with 50 mL of HPLC ethanol, then tips were dried with N_2 weak flow, and finally assembled in the Cypher ES perfusion holder, ready to perform the experiments in the AFM.

2.2 Growth, Transfer and Cleaning of Graphene Samples

2.2.1 Materials

To increase the likelihood of successful experiments, a very thin, flat and clean monolayer graphene had to be used. For this reason, a chemical vapor deposition (CVD) grown monolayer graphene on copper (Cu) was bought from Graphene Laboratories Inc. (New York, USA), or grown on copper foil used for growth the graphene, which was 35 μm thick and bought from Graphene Platform Corp. (Tokyo, Japan). The polymer used in cleanroom to protect the monolayer graphene and enabling transfer

was 495 PMMA (polymethyl methacrylate) A4, provided by MicroChem (USA). For the Cu-etching part, solution of CE-100 copper etchant from Agva Technologies Pte Ltd. (Singapore) was used, while for dissolving of copper was employed Hydrochloric acid (37 % ACS reagent grade) from Sigma-Aldrich (Singapore). For what concerns the cleaning steps (ethanol, isopropanol and acetone), performed for tip functionalization and graphene transfer, these solutions were purchased from Fisher Scientific (Singapore).

2.2.2 Transfer of Graphene Monolayer on SiO2/Si Substrate

In this section is explained how the graphene transfer was done via *chemical wet transfer* technique.[32] First of all, to get good adhesion between monolayer graphene and SiO_2/Si substrate, cleaning step of substrate wafers was performed. For cleaning step, a piranha solution was employed in order to remove all organic contaminants from wafers (300 $nmSiO_2/Si$ wafers). For the transfer's purpose, the wafers were precut 1 $cm \times 1$ cm in size. These square wafers pieces were immersed inside the piranha solution, composed of H_2SO_4 and H_2O_2 with a ratio of $70:30$, for 30 minutes with 115 °C temperature. Immediately after the piranha step, the wafers were rinsed with deionized water (DI) and sonicated for 25 minutes in order to remove the acid residues from the SiO_2 surface. In the meantime, inside the cleanroom, the first step of graphene on copper transfer was performed. In particular, graphene on copper foil was carefully cut in 3 $cm \times 3$ cm size and nestling and glue with a cleanroom-tape onto a Si support wafer. On this structure (monolayer graphene on copper foil on Si) was added PMMA and spin-coated for 70 s at 3000 rpm. Right after, PMMA-graphene-copper foil piece was baked at 150 °C for 5 minutes in order to harden the PMMA polymer on top graphene surface. Since the CVD graphene is typically grown on both side of copper foil, etching step on the bottom side of the foil was necessary to remove the unwanted part. To eliminate the bottom graphene, the copper foil was inverted upside down into a plasma machine and exposed to 2 waves of gas, one was Ar plasma (70 $W, 40$ $sccm$ Ar flow, 2.5 min) while the second was O_2 plasma (1000 $W, 40$ $sccm$ O2 flow, 5 min). When the bottom part was completely removed, copper foil was cut in 5 $mm \times 5$ mm size pieces, which were left to float on the surface of CE-100 copper etchant solution for $30 - 50$ min-

utes. When the copper was etched from all PMMA-graphene pieces, the thin polymer-graphene layers were left floating and further etching step we done in 10 % HCl and 90 % DI solution in order to remove all the possible metallic residues. Afterwards, PMMA-graphene structures were left to float in DI water to remove all remaining HCl contaminants. When 3 solutions step (CE-100, HCl and DI) were finished, graphene pieces were ready to be transferred onto target SiO_2/Si substrates. In order to ensure a good adhesion between monolayer graphene and substrate, additional baking step was done in order to remove all the water particles trapped between the two materials. Specimens were heated for 10 minutes at 80 °C, then other 25 minutes at 130 °C.

2.2.3 Cleaning and Thermal Annealing of Graphene on SiO2/Si Substrate

Once $PMMA - graphene - SiO_2 - Si$ structure is build up, deposited PMMA has to be detached from the top surface of the graphene, in order to make the graphene sample ready for analysis or experiments. PMMA removal step consisted of a 3 hours acetone bath, which is a very good selective solvent for PMMA.[33] Then samples were rinsed with ethanol and finally dried with N_2 flow. To improve the quality of the monolayer graphene and clean the sheets from particles contaminants, it was used thermal annealing at high temperatures [34]. In details, samples were initially inserted inside the annealing chamber until the vacuum pump removed air, water and reach a very low vacuum around 10^{-3} $Torr$. In next step, the chamber had to pump down to achieve ultra-high vacuum $\sim 10^{-8}$ $Torr$ so that annealing could start. Thermal annealing consists of following steps. First, temperature was ramped up from room temperature to of 350 °C for 3 hours, followed by annealing step at this temperature for additional 3 hours. At the final step, chamber was cooled down from 350 °C to room temperature for the remaining 3 hours.

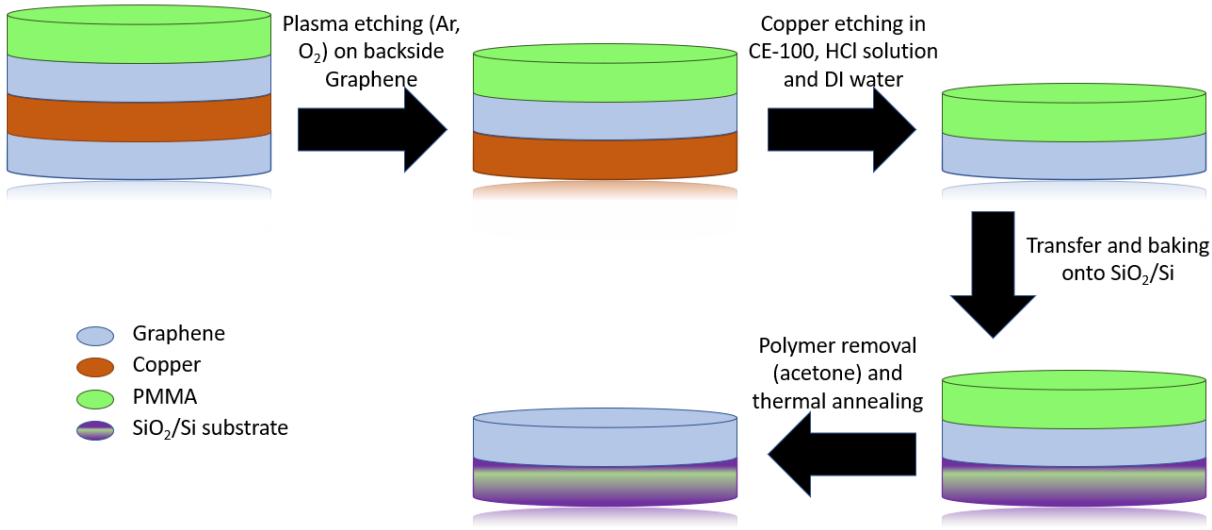

Figure 2.3: The figure represents the entire sample process. From the first step in which PMMA is stacked on the "good" part of the graphene, the second step where the backside of the "dirty" graphene is etched with the help of plasma etching, then the Cu part is removed with specific solutions and finally the sample is ready after a polymer removal and annealing step.

2.3 AFM Setup, Characterization and Evaluation Techniques

2.3.1 AFM Experimental Setup

In this section AFM setup used to explore the interaction of DNA molecules with underlying graphene surface is described. In chapter 1.2.1 there were illustrated the AFM working principle and its methods of analysis, while in section 1.2.2 it has been introduced how to calibrate AFM tip spring constant through the software program provided by the AFM manufacturers. Now attention is shifted to physical components of AFM microscope. The core of *Cypher ES* scanner is characterized from 2 essential parts: a magnetic sample stage and movable tip holder platform. On sample stage it was sticked graphene on SiO_2/Si substrate onto magnetic disc, which can be moved in horizontal direction on magnetic sample holder, while second important component is tip holder platform for the AFM chip perfusion holder, shown in Fig.2.4(b). These parts are confined inside enclosure structure that guarantees good thermal and acoustic isolation. In particular, AFM is put inside acoustic isolation box required, it is put on top of active vibration isolation platform with mechanical damping system. Acoustic and vibration isolation systems are put on top of weight dissipa-

tion platform to avoid mechanical vibrations and to distribute evenly the weight of the instrument 2.4(a).

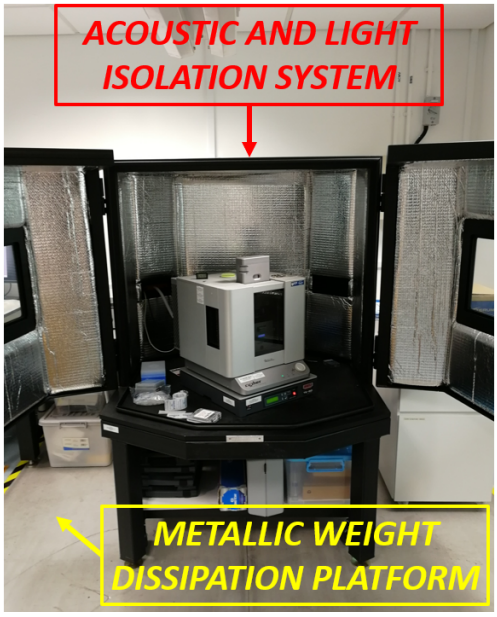

(a) Black box to avoid acoustic and light noise with a metallic platform.

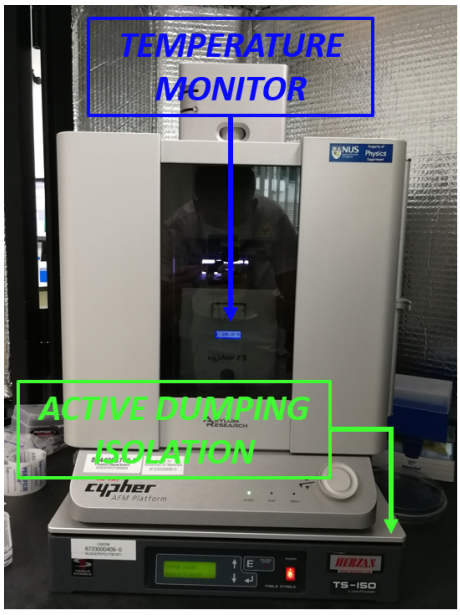

(b) Display temperature and active mechanical dumping system.

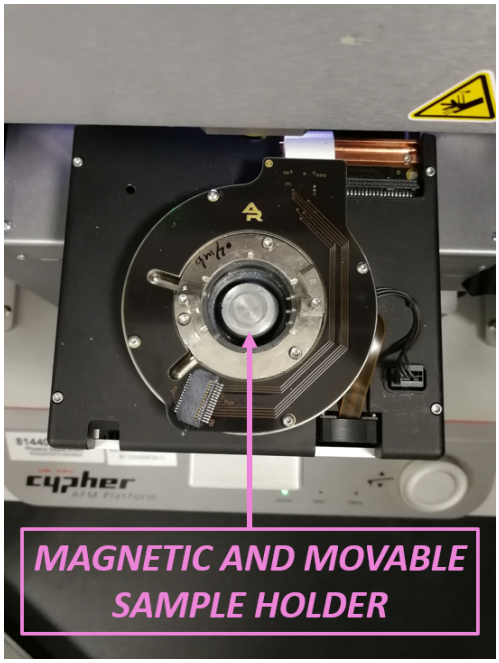

(c) Magnetic sample holder.

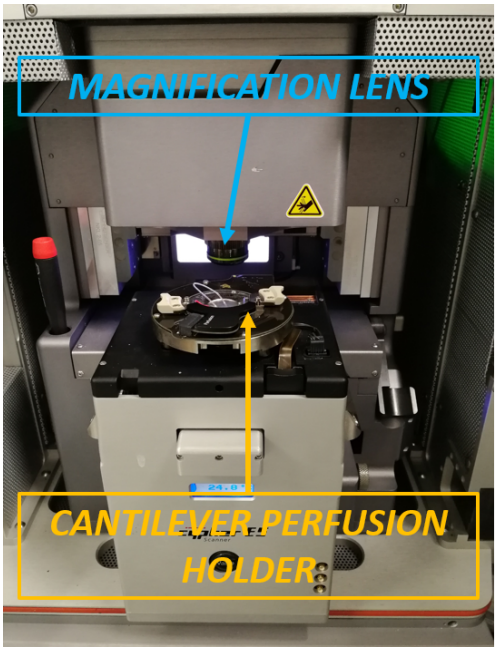

(d) Cantilever perfusion holder mounted on the AFM.

Figure 2.4: Different views regarding the Cypher ES Atomic Force Microscope.

Since the measurements performed in SMFS are very sensitive, noise reduction system is a must-have in order to increase the probability of success of the experiments. Moreover, under the magnetic movable part, AFM tool is equipped with a temperature display in which it can control the environment adjusting the temperature through a piece that uses the Peltier's principle mounted below the sample platform. As well as by means of the use of the electronic display mounted in the AFM, temperature can be managed thanks to the temperature target option implemented in Asylum's software.

Whereas the SMFM were performed in liquid environment, specific Cypher ES perfusion holder was employed, which is able to work also in liquid environment. On the quartz optical part of the holder there are two holes used to drain the liquid through two plastic pipes without affecting the quality of analyzed material, or exposing it to contaminants due to external environment such as air 2.5.

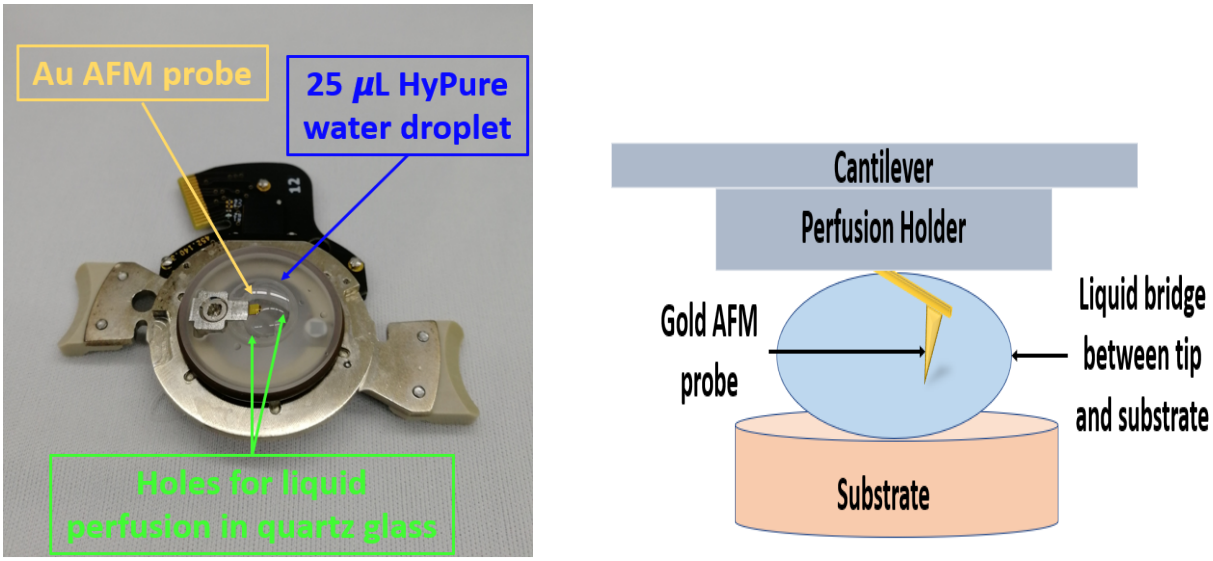

(a) Perfusion holder

(b) AFM system in liquid environment

Figure 2.5: Figure (a) points out the perfusion holes, the location of the Au tip and the HyPure water droplet to hydrate the tip, while figure (b) is a simple schematic view with the work environment ready for measurements.

When both substrate and tip are ready, graphene sample is hydrated with 25 μL of HyPure water or phosphate buffer, and positioned onto disc, and put on magnetic holder, while the AFM probe is mounted on the perfusion holder, then hydrated with 25 μL droplet and it is put upside down towards the graphene droplet. At this point, Cypher ES movable tip holder

stage is approached towards the surface with droplet forming the capillary bridge which creates the same liquid environment for both tip and sample. Once the tip and sample are close enough, AFM is locked and the noise dissipation button on vibration isolation stage is pressed in order to limit all the mechanical vibrations coming from the surrounding environment. Temperature, as mentioned above, is set with the help of Asylum software and it has to be stabilized every time before the measurements. Typically the temperature range used in these types of experiments is from 5 °C up to 65 °C and any temperature change takes 5 minutes to stabilize. Since during the SMFS experiments below 10 °C water tends to condense on other parts of setup that are not relevant for experiments, a constant N_2 gas flow is pumped for few minutes inside AFM Cypher ES body interior. Then, with Asylum software, Lorentz's peak fitting of basic oscillation mode in liquid during thermal calculation is performed, as explained in chapter 1.2.2 and InvOLS value obtained in liquid is adjusted accordingly at the chosen temperature. Once everything is set, measurements can start. Typically, to have statistically meaningful data of single-molecule peeling, at least 5 different surface position were inspected for force distance curve collection in contact mode. Typically were collected $2000 - 10000$ force vs distance curves in each experiments. Technical parameters set during the measurements were: approach and retraction velocity about 200 nm/s, 500 nm/s and 1500 nm/s, force such as tip compressive load to underlying surface was 500 pN, sampling rate of 10 kHz and low pass filter of 2 kHz. Once the measurements were finished, perfusion holder was rinsed with HPLC ethanol and tip was calibrated again to check spring constant initial and final values, discovering that these values did not differ greatly.

2.3.2 AFM Data Analysis and Evaluation for Single-Molecule Force vs Distance Curves

In this section single-molecule desorption techniques and methodologies are illustrated in order to give a general picture to the reader on how to properly explore the peeling phenomenon. When the single-molecule measurements are done, force vs distance curves are ready to be analyzed through a homemade script written with the help of the numerical computing environment MATLAB. This software is developed to ease the curves analysis,

precisely force vs distance curves are uploaded one afrer the other,and MATLAB software calculates the average force taking into account 2 nm just before the last single-molecule peeling plateau during the retraction step in force vs distance curve and subtracts it taking into account the value in which the approach and retraction behaviors provide zero force ($F = 0$), that is, they overlap, considering only 2 nm after the force jump when the tip is no touching the surface. For each curves, only the desorption phenomenon provided by the last nucleotide of the DNA chain was interacting with substrate, was considered as an analysable curve. Moreover, only only desorption distance curves that had a peeling length shorter than the total DNA oligomer length in the given experiments were taken into consideration for the data analysis.

Once the data analysis with MATLAB script is done, it is necessary to do statistic evaluation.

As mentioned in Chapter 1.2.3, force vs distance curves can show many different steps during the retraction process, and they are considered on case by case basis, where the last single-molecule desorption step in our analysis falls within constraints regarding force and step length. Let us follow example in Fig.2.6, where many different desorption steps are shown. In order to simplify the explanation, 3 different events are taken into account and they are called *event* α, *event* β and *event* γ. α is the event in which there is a single-molecule desorption from the surface, β corresponds to a concurrent desorption from the surface with two molecules involved, while γ represents a simultaneous peeling of three molecules. These 3 (or more) events are depict and characterized with their unambiguous desorption force values F_α, $F_\beta = 2F_\alpha$ and $F_\gamma = 2F_\beta = 3F_\alpha$, and interaction lengths L_α, L_β and L_γ. The desorption force or interaction length for single or multiple molecules are estimated from the tip-surface distance $z = 0$ and $F = 0$. Moreover, this length L is taken starting from the first nucleotide of the homopolymer chain that is attached to the underlying surface, up to the last nucleotide of the DNA chain that is attached to the surface.

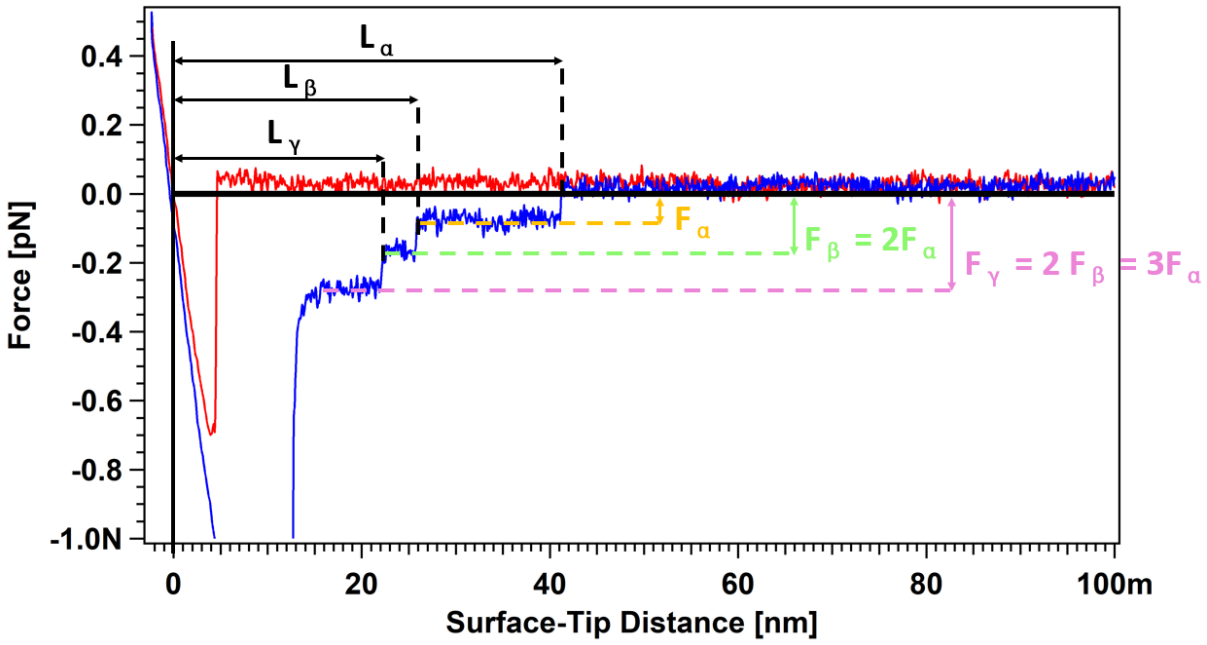

Figure 2.6: The graph represents a force vs. distance curve collected during the T-homopolymer experiment. From the graph is noticeable the different desorption length L_α, L_β and L_γ as well for the desorption force of one, two or three nucleotide at the time respectively F_α, F_β and F_γ.

Typically, most of the force vs. distance curve collected throughout the thesis project period show a single peeling step. Some portions of desorption from surface are more identifiable, as in Fig.2.6, i.e. (L_α - L_β) or (L_β - L_γ). On the other hand, parts of the force distance curve very close to jump into contact region (surface of the sample) do not show well distinguishable steps, and we cannot see the full steps. On Fig.2.6, it is shown a typical example of force vs. distance curve collected during the analysis of *thymine homopolymer* at 25 °C, where more than 3000 curves have been collected. From the total set of collected of curves, only 277 have been taken into account because most of the remaining curves presented had a too high jump in force value, or did not have uniform peeling force step. To obtain consistent statistical inference, total amount of selected useful curves had to be at least 200, and data was plotted in histograms as the total number of force curves vs the single-molecule desorption force values, as shown in Fig.2.7. All results for forces obtained during the desorption force experiments will be given in the structure of "mean(average) force value(F_0) $\pm$ total measurement error(ΔF)". The *mean(average) force value (F_0)* is the term that corresponds to the peak position in histogram value obtained

from the experimental force histogram by applying the Gaussian nonlinear distribution fit in equation 2.3. In all desorption force histograms, on the y-axis we have number of force vs. distance curves with for certain single-molecule desorption force, while on the x-axis we have numerical value of desorption forces. Moreover, typical size of the bin used in histogram is 1.5 pN. To perform statistics on the single-molecule desorption forces, values are fitted with the Gaussian distribution:

$$F = F_0 + Ae^{-\frac{(F-F_0)^2}{w^2}} \tag{2.3}$$

where F_0 is the Gaussian peak position, A is the amplitude of the Gaussian, w is the width of the Gaussian at half maximum, while F is the experimental desorption force value measured. Furthermore, the standard deviation of the Gaussian peak δF was used as a fitting error. Recovering the example of the *T-homopolymer* experiment at 25 °C, peak desorption force obtained is $(70.76 \pm 0.27)pN$ while the amplitude is $(57.28 \pm 1.46)pN$.

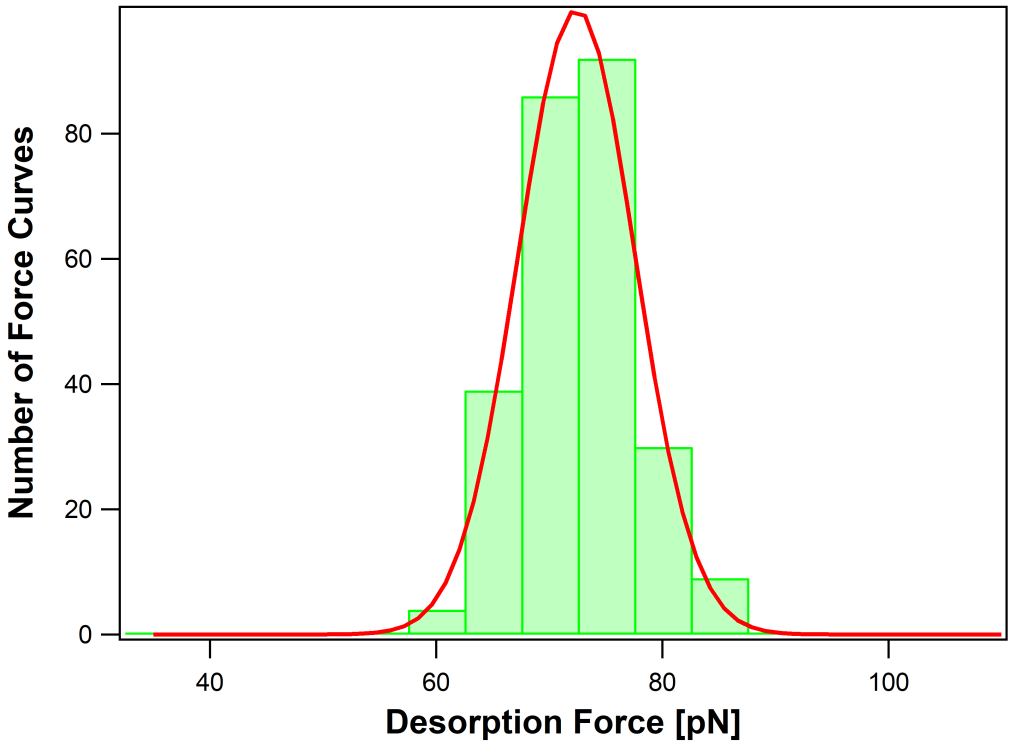

Figure 2.7: The graph represents a force vs. distance curve collected during the T-homopolymer experiment at 25 °C. Force vs. distance curves considered in this experiment were 277 with a peak force of $(70.76 \pm 0.27)pN$.

2.3.3 AFM in Tapping Mode and Optical Microscope Imaging

In this section are illustrated the characteristics and parameters used to obtain graphene images via 2 different methods: AFM tapping mode and optical microscope imaging. Moreover it will also be shown the substantial difference between a clean and contaminated sample. For both instrumental analysis, graphene samples were prepared with procedures explained in Chapters 2.2.2 and 2.2.3. These 2 microscope tests had been adopted in order to figure the cleanliness out, because contaminants in graphene sample might negatively affected the outcome of experiments. Details regarding *AFM tapping mode* have already been explicated in Chapter 1.6 and Fig.2.8 represents a portion of graphene sample. Typically, thanks to tapping technique, it could be possible to achieve an atomic resolution of specimen. Resolution is limited by the AFM probe curvature radius. Overcoming this limit, the sample resolution became a trade off between scan size and number of points and lines selected during raster scanning in x-y direction:

$$Resolution = \frac{Scan\ Size}{Points\ \&\ Lines} \tag{2.4}$$

Sample surfaces were analyzed in order to discover clean areas for use in our experiments, and from our data we found out that the annealing process worked well and that large percentage of the surface area was always clean. AFM measurements and image collection was done with scan rate of 2 Hz, scan size of 20 μm, 512 points and lines, amplitude oscillation set point of 300 mV and an integral gain of 30 it was reached an acceptable resolution as shown in Fig.2.8. Usually area of 20 $\mu m \times 20\ \mu m$ was analyzed, but for the sake of interest and knowledge of this project, a smallest area of 5 $\mu m \times 5\ \mu m$ was selected to identify more surface features. From these images one can identify the roughness of the surface and the quality of the transferred graphene overall.

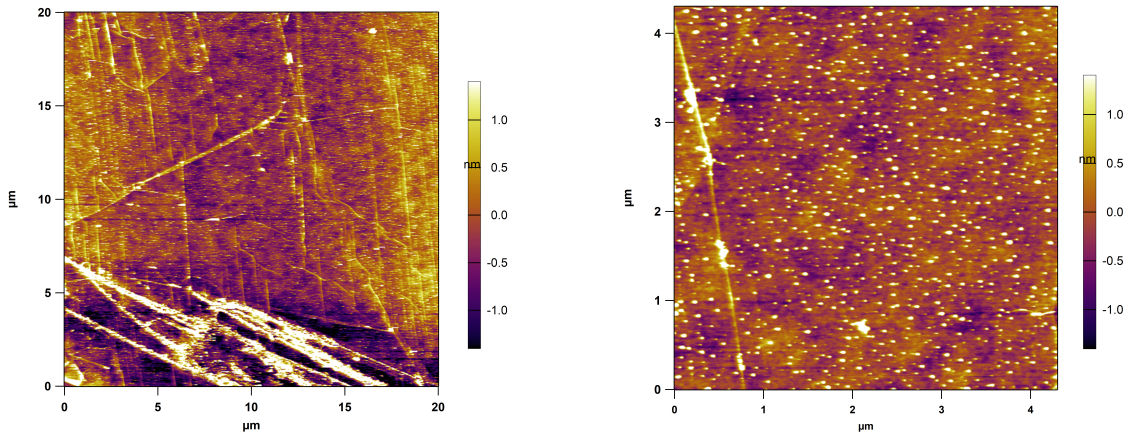

Figure 2.8: The images represent the graphene surface with a focus area in height retrace mode of 20 $\mu m \times 20\ \mu m$ on the left side and 5 $\mu m \times 5\ \mu m$ on the right side.

On the other hand, with the help of a classical optical microscope it was very simple to visualize samples with contaminants, and compare them with annealed, clean samples. As well, it was quite easy to check continuity of our transferred graphene monolayer films. The images were taken both in bright and dark field. For both annealed and non-annealed images we used a magnification of 5×, 10× and 50×. In particular, pollutants on surface could be the result of a transfer process, PMMA residues, metal residues from copper foil or even presence of silicon splinters as in Fig2.9. In contrast to this, samples after annealing show very small of contaminants and majority of surface is clean, as seen from Fig.(b), (d) and (f) 2.9.

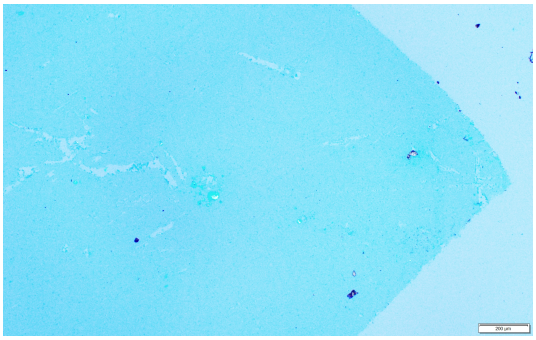

(a) 5× magnification in bright field non-annealed sample

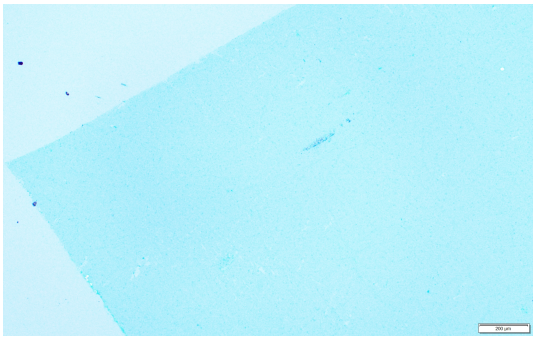

(b) 5× magnification in bright field annealed sample

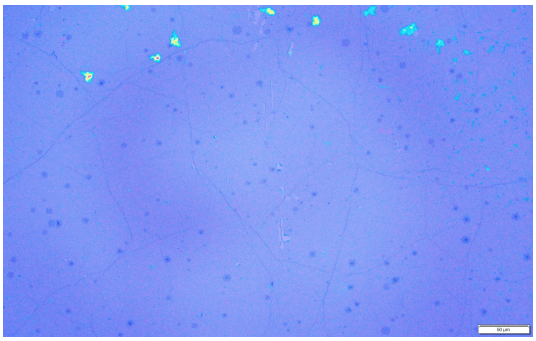

(c) 20× magnification in bright field non-annealed sample

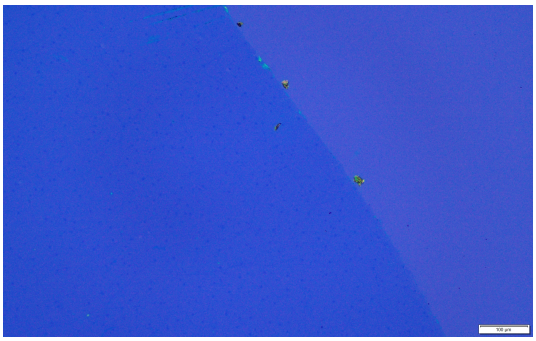

(d) 10× magnification in bright field annealed sample

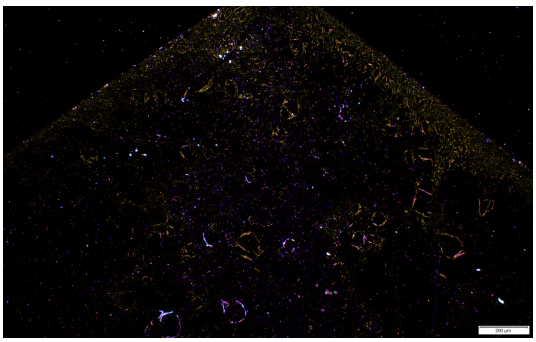

(e) 5× magnification in dark field non-annealed sample

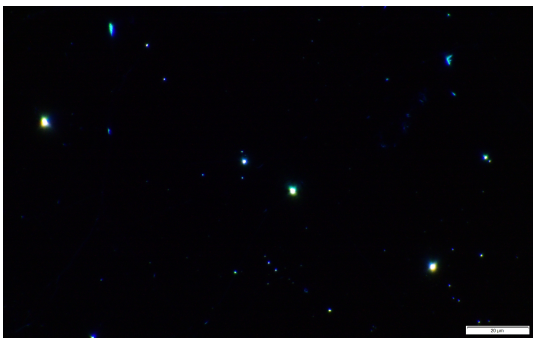

(f) 50× magnification in dark field annealed sample

Figure 2.9: Comparison between non-annealed and annealed samples. In figure (a), (c) and (e) contaminants occupy the large amount of graphene surface, while (b), (d) and (f) after annealing present a cleaner surface with very few contaminants limited in certain spots.

2.3.4 Raman Spectroscopy

In this section we give a brief overview and principles of textitRaman spectroscopy. We used this technique to determine quality of transferred and annealed monolayer graphene samples. This method was named after Indian physicist, *Sir C. V. Raman*, who discovered how the light undergoes a scattering phenomena inside the material, and how some of the reflected or transmitted light can be changed in amplitude and wavelength upon exiting from the sample. This light effect is called *Raman scattering*. Since this discovery, Raman spectroscopy has been able to apply in many different fields, to recognize types of chemical bonds in materials, which is useful in chemistry, for material characterization, for temperature and crystallographic orientation analysis in solid state physics, foe studies of biological functions in biology and medicine, and even for applications in detection of explosives.[35] Raman spectroscopy produces extremely accurate results without damaging the analyzed sample, providing information about structural and electronic proprieties of materials. This advantage makes Raman spectroscopy suitable for 2-D materials characterization.[36] Raman spectroscopy in graphene provides us with useful information regarding electronic properties, such as level of electron doping, electron mobility and others.[37,38] Raman spectroscopy setup starts with a source of monochromatic light that impinges the material. Photons in the laser beam interact with the molecular vibrations modes, phonons, or other excitation in the system causing change in the incident photon's beam energy. The resulting energy shift of exit beam allows us to obtain substantial information about the phonon and/or electron modes inside the system. Reflected and transmitted photons of laser beam, after initial beam is directed to the surface, are directed towards a lens which collects the light, which is filtered by a notch filter, and finally collected on the CCD camera chip. This technique is very selective to the choice of wavelength that impinges the sample, and the filter used to process data from collected light. In other words, if the frequency of the photons emitted from the sample is equal to the frequency of the laser beam we have a typical *Rayleigh (elastic) scattering*, $\nu_{final} = \nu_{initial}$ so the light is filtered out. Otherwise, when scattered photons have different energy compared to the initial laser beam, we have *Raman (inelastic) scattering*, with different initial and final frequencies,

$\nu_{final} \neq \nu_{initial}$, and the light passes through the notch filter. Difference in frequencies comes from the interaction between incident photons with the material phonons. Since the emitted photon energy could be greater or lower than laser beam, when the frequency of inelastic photons is higher than incident light, and in the spectrum we will see *Anti-Stokes lines*, while if emitted photons are at lower energy than incident light, the spectrum shows the *Stokes lines* as appear in Fig.2.10.

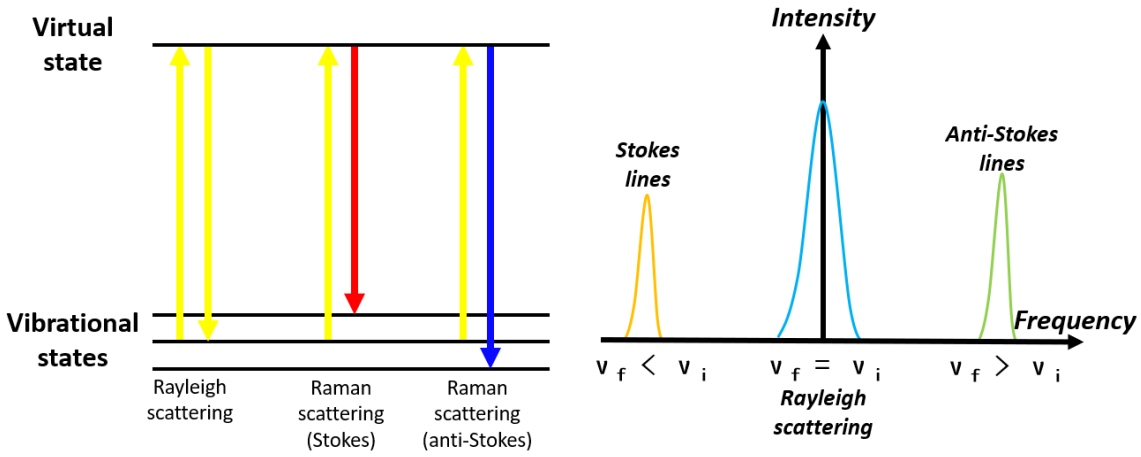

Figure 2.10: The images represent the graphene surface with a focus area in height retrace mode of 20 $\mu m \times 20$ μm on the left side and 5 $\mu m \times 5$ μm on the right side.

3 Physical Interaction between Functionalized Au-Tip and Graphene Surface

In this chapter we present our measurements and describe what happens during DNA surface interaction at their interface. In this thesis we use novel approach to develop a model which roughly describes how the DNA behaves in proximity (contact) of graphene substrate. Particular effort is put in explaining effect of interfaces that play an essential role in this interaction model, such as DNA-liquid interface, liquid-surface interface and DNA-surface interface. A lot of information on interfaces can be obtained via contact angle measurements, which we also present here. We present here the whole data collected during the thesis project period, with emphasis that different ssDNA homopolymers (A, C, T) were used in experiments. For the first time ever, we explain in details how temper-

ature can affect hydrophobicity of the analyzed molecules near substrate surface, and how that uncovers the true nature of interactions. To start, lets define major interactions that generally occur in similar analyses between polyelectrolytes and surfaces in SMFS experiments. Interactions are generally divided in *electrostatic* interactions and *non-electrostatic* interactions. First type of interactions can be affected when there is change in liquid environment, such as change in pH, where we add excess positive or negative ions, thus affecting the range and magnitude of electrostatic interactions and amount of effective charge. As well changes is added NaCl concentration from low to high values can affect the range of electrostatic interactions which involves electrostatic charges or static dipoles (higher amount of NaCl means that interactions are screened more effectively and electrostatic part of interactions is weaker). These are usually interactions that involve interaction of phosphate backbone with underlying graphene. On the other hand, non-electrostatic interactions include types of interactions of DNA and surface where we don't have static charge distributions. Best example of these are vdW dispersive interactions. For example, important study by Manohar et al.,[11] in which they did SMFS of various homopolymers (A, C, T) on HOPG, which involved changes in salt (NaCl) concentration in their aqueous and buffer environment, brought them to conclusion that the average desorption forces are independent on molarity of added NaCl, therefore interactions are not electrostatic in its nature. In literature, authors have tried to change electrostatic proprieties in order to identify which parameter and forces can affect the desorption forces behavior of other polyelectrolytes interacting with other surfaces, coming to similar conclusions. In the case of this thesis, we inferred from our measurements that contribution provided by electrostatic interactions was negligible. Based on this experimental conclusions, non-electrostatic interactions and hydrophobic interactions are ones that might dominate the physics behind oligomers-surface interaction.[39,40] Starting with these assumptions, in the next chapter, 3.1, we check these claims and try to explain in detail how do our measurements respond to these assumptions.

3.1 Physical Meaning of Interfacial Free Energy

Purpose of this section is to find alternative approach to correlate temperature and interfacial free energy chenges in order to extrapolate data regarding the non-electrostatic interaction (*van Der Waals* dispersive or $\pi - \pi$ stacking interactions) and possibly for *hydrophobic interaction*. As introduced in Chapter 3, the main interactions involved in a ssDNA/graphitic system are provided by electrostatic, non-electrostatic and hydrophobic. In order to retrieve a plausible model to describe the interactions of polyelectrolytes and hydrophobic surface, such as graphene, the electrostatic interaction can be considered negligible since it provides a much smaller value compared to the value of other interactions in the system. Papers produced by Suresh Manohar et al. as well claim that the major component of the binding free energy between biological material and graphitic surfaces is brought by non-electrostatic contributions, as well as hydrophobic interactions, but they don't provide any experimental evidence.[11] From now on, we assume that the main forces in our model are van Der Waals and hydrophobic. With help of the mathematical development provided by my supervisor in his previous work,[22] we write total desorption force F as an adhesion force:

$$F = F_{adh} + F_{entropic} \tag{3.1}$$

where the total adhesion force F_{adh} can be considered as a sum of two individual contribution provided by hydrophobic attraction due to hydrophobic hydration of hydrophobic nucleobases of homopolymer, and hydrophobic monolayer graphene, while the second contribution is due to the pi-pi interactions formed between aromatic nucleobases of A,C and T homopolymers and the monolayer graphene. So equation 3.1 can be rewritten as:

$$F = F_{hyd} + F_{\pi-\pi} + F_{entropic} \tag{3.2}$$

where F is average desorption force of ssDNA from graphene, F_{hyd} is the total interaction due to hydrophobic attraction of DNA molecules and graphene, $F_{\pi-\pi}$ is the total interaction due to $\pi - \pi$ stacking interaction,[41] while $F_{entropic}$ is the contribution of the desorbed part of the polyelectrolytes chain. Extrapolating some insight from the work of my colleague, two parameters from the total force contribution can be neglected since their contribution do not offer a significant change in the physic of the

system. These term are $F_{\pi-\pi}$ and $F_{entropic}$ which provide a contribution of $10-20$ % and $5-10$ % of the total force contribution, respectively.[22] The largest contribution, 70 %, of the total interaction is due to F_{hyd}. This is an important result in understanding the physic of the system because points out how hydrophobic hydration and hydrophobic interaction are the key interaction factors in the system composed by ssDNA homopolymers and monolayer graphene. This is especially important in application.

After this brief explanation that had shown the importance of hydrophobic interaction, it is crucial to understand what interfacial free energy means. In a simplistic way it can be defined as the energy required to wet the surface per unit area $\gamma = \frac{\delta E}{\delta A}$, but in a deeper explanation, interfacial free energy contains much more complicated concepts. *Interfacial free energy* quantifies the energy releases in the system when a new surface is created, this means when 2 surfaces approach each other, the bonds in the water-substrate interface are broken and there is a release of energy to exploit thanks to the break. If this energy released is high means that this energy has not been absorbed to create new interface bonds (hydrophilic interaction), resulting in a high value of interfacial free energy therefore hydrophobicity. Otherwise if the resulting interfacial free energy is low means that there is an increase of interface area, so the energy has been absorbed to create new interface bonds, therefore hydrophilicity. At this point, after giving the above definition and consideration of interfacial energy, it is possible to derive a model which includes wettability and consequently, hydrophobic interaction. Total variation of interfacial free energy in our system (per nucleotide) includes contribution of three terms:

$$\Delta\gamma = \gamma_{g-w} + \gamma_{d-w} - \gamma_{g-d-w} \tag{3.3}$$

where $\Delta\gamma$ is the difference between interfacial energies made by unbound and bound states. Unbound state is when nucleotide and graphene surface are not in close contact, while bound state means nucleotide and surface tied together. γ_{g-w} is the interfacial energy between graphene substrate and HyPure water + buffer solution, when DNA is far away and it can not disturb the graphene-solution interface. γ_{d-w} is the interfacial energy between DNA and experimental solution, when graphene surface is distant from the DNA-solution interface. γ_{g-d-w} is the interfacial free energy corresponding to the interface created when DNA and underlying graphene

are in strict direct contact inside the liquid. The sum of the two terms, γ_{g-w} and γ_{d-w}, coincide with the initial state of the system, when DNA and graphene are far away from each other. On the contrary γ_{g-d-w} corresponds to the final state when nucleotides and graphene interact together. Further consideration have to be made to unravel and understand the three terms in equation 3.3. All the three are made up with specific values based on the role they play in the system, for example γ_{g-w} contains within it the value corresponding to the surface energy of graphene. On the other hand, both γ_{g-w} and γ_{d-w} contains two constant terms, the surface tension of liquid and the contact angle value. The latter is very often used during the evaluation of wetting proprieties of surfaces.[42] Some of these proprieties could be synthesized as interfacial tension between liquid and solid interface, static contact angle and many others.[43] Knowing the static contact angle for the purpose of our experiments, it is trivial to connect each terms of equation 3.3 with the Young's equation[44,45] :

$$\sigma_{s-v} = \sigma_{s-l} - \sigma_{l-v}\ cos\alpha \tag{3.4}$$

where σ_{s-v} is the surface tension between solid and vapour environment, σ_{s-l} is the surface tension between solid and liquid interface, σ_{l-v} is the surface tension between liquid and vapour environment and α corresponds to the static contact angle on boundary of three phases. Vapour phase is typically taken as air environment and is omitted from indexing. Equation 3.4 for the purpose of the thesis considerations can be rewritten, so we can calculate term γ_{g-w} from equation 3.3:

$$\gamma_{g-w} = \sigma_g - \sigma_l\ cos(\alpha_{g-w}) \tag{3.5}$$

where σ_g is the surface energy of graphene and it does not change with a temperature variation, σ_l is the surface tension of liquid and α is the static contact angle. For what concern the term γ_{d-w}, it was made an assumption regarding the gold tip-dna-water interface, considering the interaction only between DNA and water solution, concluding with the following equation:

$$\gamma_{d-w} = \sigma_d - \sigma_l\ cos(\alpha_{d-w}) \tag{3.6}$$

where σ_d is the surface energy of DNA on gold in air, while the terms σ_l and α are surface tension of liquid (approximately water) and contact angle,

respectively. Further approximation has to be made for the last term of equation 3.3 in which it was considered that DNA covers half of graphene surface (once they interact), producing the following result:

$$\gamma_{g-d-w} \simeq \frac{1}{2} \cdot (\sigma_{g-w} + \sigma_{d-w}) \simeq \frac{1}{2}\, \sigma_{g-d} \tag{3.7}$$

In Chapter 4, there will be presented and explained results obtained via calculations with above formulas with our experimental data. Particularly interesting will be understanding of how the hydrophobicity affects the slope of the average desorption *force vs total interfacial free energy difference* graph and how the van Der Waals interactions can be found from the graph in limit when $\Delta\gamma$ goes to zero, or in better words, without liquid environment, with $\sigma_l = 0$.

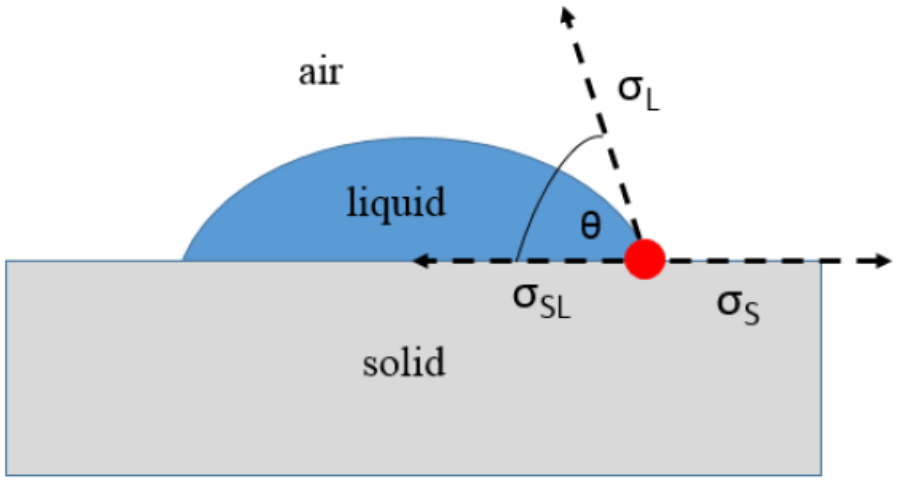

Figure 3.1: Representation of the force components at the three phase boundary. Surface tension components are denoted with σ_{SL} which is the interfacial tension between the solid and liquid phase, σ_S is surface tension between solid substrate and environment while σ_L is surface tension between liquid phase and environment. Static contact angle value in equilibrium is labeled with θ.[22]

All experimental quantities which depend on temperature, such as total interfacial free energy, graphene-water contact angle and DNA-water contact angle, are explained through specific graphs and tables in the Chapter 3.6.

3.2 Experimental Procedure

This section is made to show the procedure used for the following experimental sections. With this specific procedure it was possible to collect useful data, and in future CA2DM researchers will be able to deepen and develop a more solid theory in which there will likely explain all details on nature of interaction of biological material with 2D substrates. All the material mentioned in this section are cited in Chapter 2.

Before handle AFM probes, DNA, or graphene, we prepare phosphate buffer solution of 10 mM concentration and 7.2 pH. Then we prepare Au tips with DNA. This step was one of the trickiest, because DNA attachment on tip is quite sensitive on external perturbations, or any wrong concentrations of ingredients in modification solutions. Briefly, AFM probes were inserted in plasma machine to clean contaminants on them, in the meantime DNA was diluted from 100 μM to 0.3 nM in order to allow the adhesion with gold tips. Then 0.3 nM DNA solution and cleaned gold tips were immersed together with TCEP and later with the 6-MHA in ethanol. 2D substrate preparation was made in cleanroom. Graphene on copper foil was cut, spin coated, etched on backside by plasma machine then wet etched with proper solutions. Once ready, very thin foils of graphene were transferred on a Si/SiO_2 supporting substrate. Cleaning step (annealing) was performed on the graphene substrate sample in order to enhance the adhesion and remove contaminants. The next step was put gold tip and graphene substrate on their holders with 25 μL of buffer solution, in order to start the experiment with Atomic Force Microscope. When experiments were completed, the data analysis was performed with software environments of Matlab, Python and Igor Pro.

As mentioned in the beginning of this section, all the details concerning the techniques are widely described in the dedicated chapters and this was just meant to be a short description to remember the procedures before starting to describe the different experiments carried out in this thesis.

3.3 Nature of ss-Adenine Homopolymer Interaction with Graphene Substrate

This set of experiments takes into account a homopolymer chain composed by a nucleotide called *Adenine*. This base is made of carbon, nitrogen and hydrogen atoms with a chemical formula $C_5H_5N_5$ 3.2. As mentioned in Chapter 1.1, nucleotides are divided in 2 categories: purines and pyrimidines. Substantial difference between these 2 categories is based on their structure. Purines contain a six-membered nitrogen-containing ring fused to an imidazole ring whereas pyrimidines contain only a six-membered nitrogen-containing ring.[46] Adenine is the largest base and we expect it to manifest a higher hydrophobic behavior in liquid once temperature changes, relative to thymine and cytosine.[47] Manohar et al. have discovered the peeling force needed to a polyadenine chain to detach a single molecule from a graphitic surface and this force corresponds to $76.6 \pm 3.0\ pN$.[39] Since the substrate they used was graphite and not graphene as in our case, we expected a slightly different result compared to the one obtained by Manohar et al. at room temperature, however we expect a peeling force in the same order of magnitude.

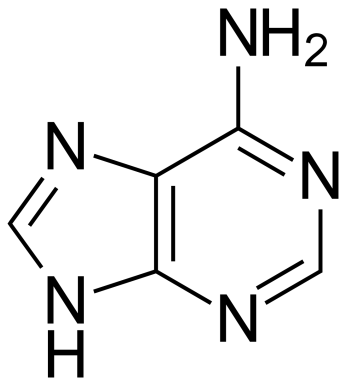

Figure 3.2: Molecular representation of adenine nucleotide with the aromatic structure fused with the imidazole ring.

3.3.1 Data Analysis and Results

In order to obtain significant data for our analysis, we have collected a large amount of force vs distance curves, changing both temperatures and loading rate inside the AFM setup. We changed the tem- perature from

5 °C, 10 °C, 15 °C, 25 °C to 35 °C, in order to analyze the hydrophobicity and total interactions of the adenine homopolymer with monolayer graphene. Loading velocity has been changed from 200 nm/s, 500 nm/s to 1500 nm/s in order to understand how the change of loading rate could affect the DNA-graphene interaction. Data collected has been taken during continuous approach and retraction of A-homopolymer coated Au tip from the underlying graphene surface in z direction, with the speed set for that particular experiment. With the help of Fig.3.3 we see total length L of all the nucleotides attached with covalent bond to the Au tip that interact to the graphene surface. In total lenght L we include dual contribution provided by the nucleotides adhered to the surface L_{adh}, and the nucleotides already desorbed from the graphene, L_{des}. While Δz_0 is the offset distance relative to tip apex where DNA molecules covalently attach.

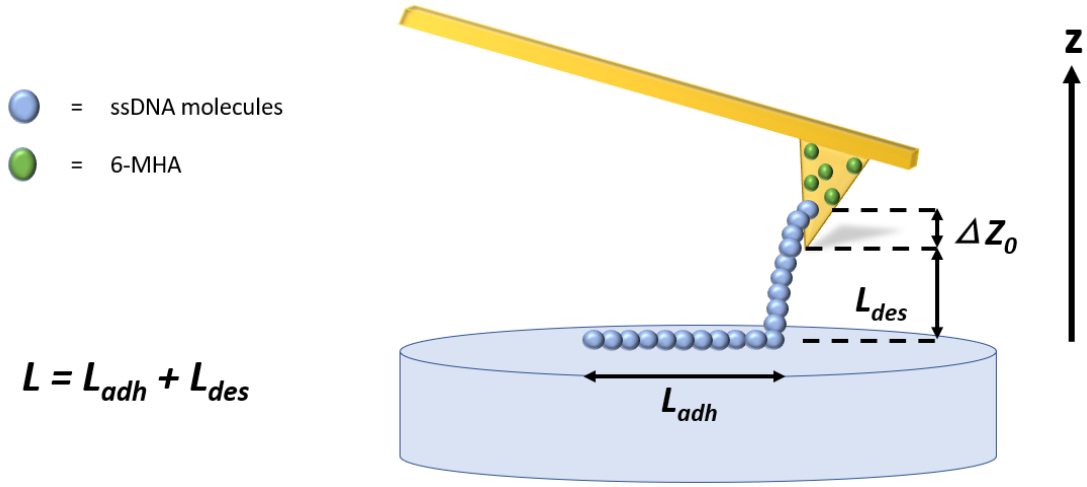

Figure 3.3: Graphic representation of the total length during approach ($-z$) and retraction (z) process between AFM probe and underlying surface.

When the tip with tied ssDNA molecules is approaching the graphene surface, event of jump-into-contact occurs typically in z-direction above the graphene surface at a distance of $2-15$ nm. This phenomenon agrees with several author in literature with graphitic surfaces, saying that jump-into-contact happens because of the simultaneous attachment of several ssDNA homopolymers on graphite via non-electrostatic interaction (pi-pi stacking and hydrophobic interaction) of hydrophobic, aromatic, ssDNA nucleobasis with the below surface[39,40] . On the other hand, when retraction mechanism begins, a large non-specific adhesion appears, probably due to same

reason for which jump into contact happens. When the physical contact between tip apex and graphene is broken, as shown in Fig.3.3, only few DNA molecules are still located on the graphene surface (L_{adh}) and a desorption plateau (single-molecule desorption) occurs if the density of DNA molecules is quite low. As mentioned in Chapter 2.3.2, a single-molecule desorption event means a nucleotide-by-nucleotide detachment from the graphene surface in a equilibrium condition.

Data collected have been meticulously analyzed to see if the experimental procedure was performed correctly in order to achieve force vs distance curves with a significant force jump during AFM retraction process. In the following Table 1 is represented the total number of force vs distance curves, the total curves collected with force jumps and the force vs distance curves taken into account for the analysis. Sometimes, peeling force steps are not present in any of the collected curves during the experiment, sometimes curves have peeling force jump values which show some anomalies such as too high force due to surface contamination, or a force jump with acceptable value but with peeling length much longer than expected adenine homopolymer length, or many other irregularities as explained in Chapter 1.2.3. In order to have statistically meaningful samples of evaluated force vs distance curves, we took a minimum value of 200 curves to a maximum value of 350. In the Table 1 below we report only the temperatures used during the experiment without considering the total number of gold tips employed to collect the data at given temperature. This is because in some cases AFM probe could break or not work well, but more than one AFM tip may have been used to collect these data. This was possible because all the data collected have been adopted the same configuration of tip with similar spring constants and same loading rate of $500 nm/s$.

T [°C]	T [K]	Total curves collected	Total curves with force jumps	n° of curves used for analysis
5	278.15	7226	5058	2300
10	283.15	8059	6447	629
15	288.15	10191	8152	680
25	298.15	7462	5969	3272
35	308.15	7117	5693	2135
TOTAL		33339	26189	9016

Table 1: The table represent the data collected with different temperatures with a fixed loading rate of 500 nm/s.

The following desorption force histograms show the data collected during the adenine single-molecule desorption experiment for each temperature employed. In histograms is possible to see how the data collected are well fitted with Gaussian statistics. In particular, from equation 2.3, it is possible to notice how the Gaussian peak position $F0$ matches perfectly with the average desorption force of individual adenine homopolymer.

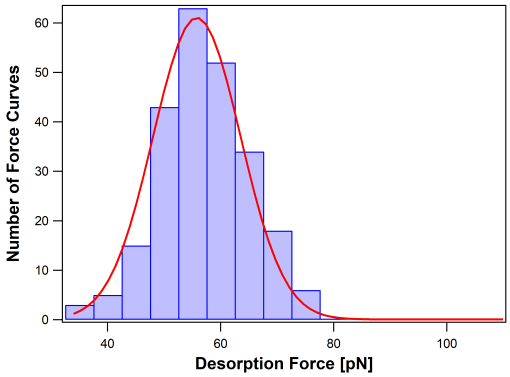

(a) Desorption Force at 5 °C

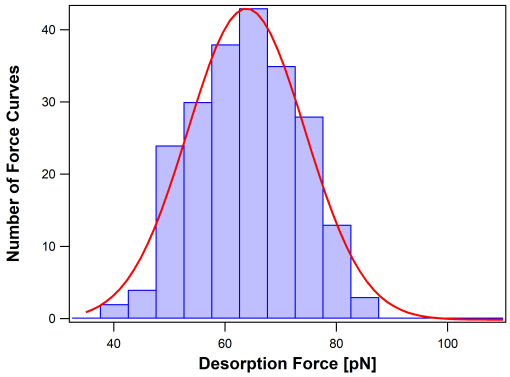

(b) Desorption Force at 10 °C

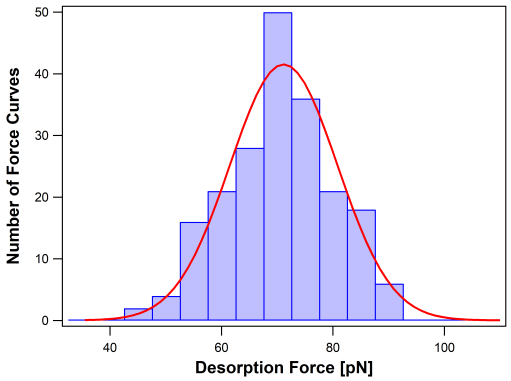

(c) Desorption Force at 15 °C

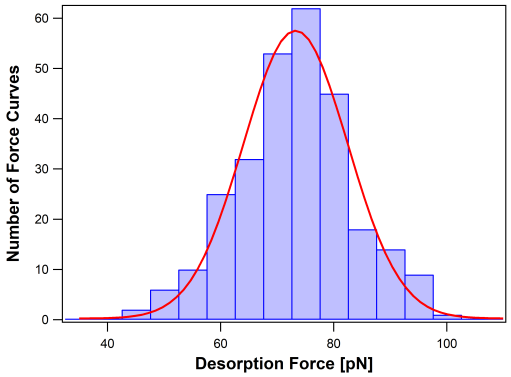

(d) Desorption Force at 25 °C

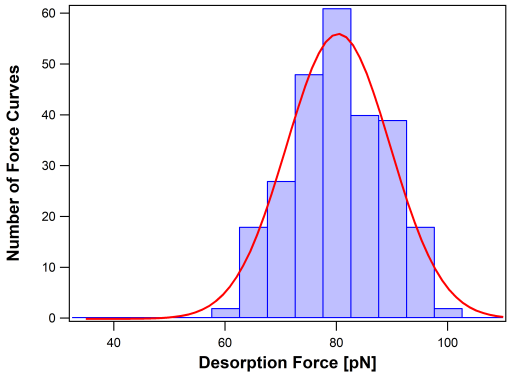

(e) Desorption Force at 35 °C

Figure 3.4: Force histograms obtained during the single-molecule force spectroscopy experiments on graphene surface. Histogram in (a) represent experiment with 5 °C environment, (b) experiment in 10 °C condition, (c) with a temperature of 15 °C, (d) at 25 °C, while (e) are data collected in 35 °C condition. The red line in all the figures is the Gaussian fitting with a formula used in equation 2.3.

Value obtained for each temperature experiments are the following, with temperature increasing order from 5 °C to 35 °C as in Fig.3.4:

- for 5 °C, 239 curves considered with desorption force peak in (54.306± 0.135) pN and a Gaussian amplitude of (61.007 ± 0.935) pN
- for 10 °C, 220 curves considered with desorption force peak in (61.349± 0.248) pN and a Gaussian amplitude of (43.108 ± 0.892) pN
- for 15 °C, 202 curves considered with desorption force peak in (68.164± 0.368) pN and a Gaussian amplitude of (41.499 ± 1.39) pN
- for 25 °C, 277 curves considered with desorption force peak in (70.764± 0.267) pN and a Gaussian amplitude of (57.278 ± 1.46) pN

- for 35 °C, 255 curves considered with desorption force peak in (77.855± 0.277) pN and a Gaussian amplitude of (56.067 ± 1.46) pN

From the above data, it is visible how the force jump is shifted to higher values with a increase in temperature. This result was expected, according to the hydrophobic hypothesis, but to analyze in details the effect of temperature, reader is redirected to section 3.6 because many other parameters have to be taken into account.

In order to better understand the mechanism behind the desorption of single nucleotides from graphene surface, we additionally changed the loading rate (multiple of spring constant and velocity) to characterize the free energy landscape. The purpose of switching the loading velocity from the standard value of 500 nm/s is needed to realize if desorption is an equilibrium or non-equilibrium process. In order to cover a wide variety of loading rate points, we used additional other 2 velocity during the analysis. These loading rates were at 200 nm/s and 1500 nm/s. In the following Table 2 we represent the total number of curves collected during the experiments. There is a significant difference between the total number of curves collected at 500 nm/s and the other two loading rate because the aim of the thesis was focused on the analysis of temperature dependence.

T [°C]	**T [K]**	**Total curves collected with 200 nm/s**	**Total curves collected with 500 nm/s**	**Total curves collected with 1500 nm/s**
5	278.15	1751	7226	2241
10	283.15	1973	8059	2326
15	288.15	2192	10191	2505
25	298.15	940	7462	2532
35	308.15	2052	7117	3958
TOTAL		8908	33339	13562

Table 2: Table represents the number of curves collected for each loading rate, 200 nm/s, 500 nm/s and 1500 nm/s.

Moreover, change in loading rate is macroscopically visible during the force vs distance curves collection because curves taken with 1500 nm/s have lesser points and lower noise during the approach and retraction, and force jumps are less clear. On the other hand, with 200 nm/s steps are

very clear and stable but the environmental noise is more pronounced as shown in Fig.3.5.

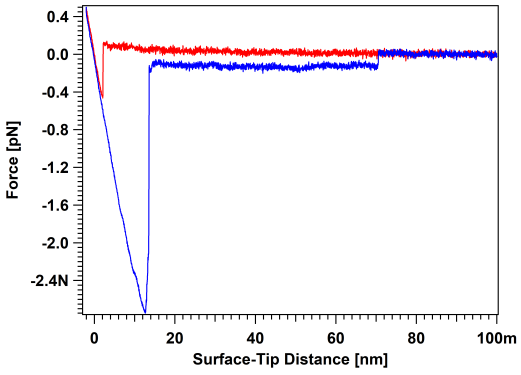

(a) Force vs distance curve at 200 nm/s

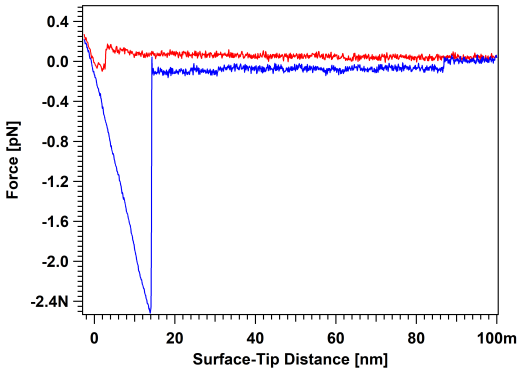

(b) Force vs distance curve at 500 nm/s

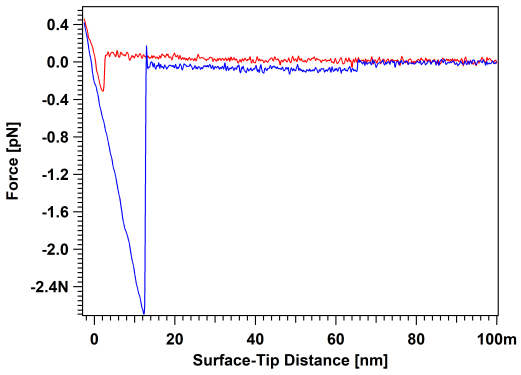

(c) Force vs distance curve at 1500 nm/s

Figure 3.5: The three images are force vs distance curves taken at 5 °C with 200 nm/s, 500 nm/s and 1500 nm/s. In figure (a) the most pronounced trait and noise during approach/retraction are notable, while in (c) the trait is thinner with less noise.

All the data obtained in this section will be discussed and compared in the specific chapters, 3.6 and 4.

3.4 Nature of ss-Cytosine Homopolymer Interaction with Graphene Substrate

In this section the focus will be on another type of homopolymer chain called *Cytosine*. Also the nature of this base is made by carbon atoms (4) and nitrogen atoms (2) centered in position 1 and 3 inside the pyrimidine 6-membered ring and hydrogen atoms Fig.3.6. Its chemical composition is

$C_4H_5N_3O$. As mentioned above, cytosine is part of the family of pyrimidines. In literature, cytosine is mentioned as the smaller base, with a great affinity to create a bond thanks with its major number of hydrogen atoms than the other bases and it should have a weaker hydrophobic character compared to the other bases.[47] Consequently, cytosine should show a less pronounced dependence on temperature of liquid compared to the other bases, presenting a less steeper slope in the final force vs temperature analysis compared to adenine. A Manohar et al. measured the peeling force needed to peel a polycytosine chain from a graphitic surface of $60.8 \pm 5.5\ pN$.[39] In the same temperature condition, we expected a peeling force from graphene to be similar, at least in order of magnitude, to the value mentioned.

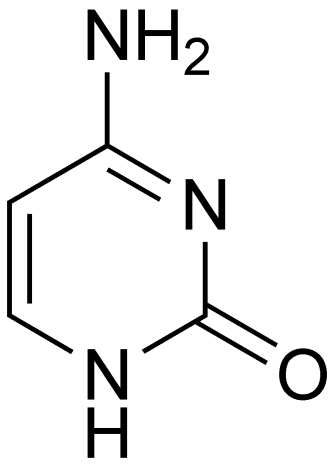

Figure 3.6: Structural representation of cytosine molecule with the amine group in carbon C4 and a keto group in the carbon C2 forming a pyrimidine ring.

3.4.1 Data Analysis and Results

Force vs distance curves collected from our experiments are collected at different loading rates and applied temperatures to understand how the total interaction between cytosine and graphene is affected. Loading rate was changed from a standard configuration of 500 nm/s to a smaller velocity of 200 nm/s, and then higher velocity value of 1500 nm/s. Temperature was changed from 5 °C, 10 °C, 15 °C, 25 °C to 35 °C. The mechanism of AFM probe approach and retraction is explained in Chapter 3.3.1 and it was also used for the cytosine experiment. In this case, the results analysis

is divided into several parts because the cytosine, adenine, and thymine with were measured by me for graphene on SiO_2/Si substrate, while other type of substrates were used by my mentor in his previous experiments, and these graphene substrates are gold, silicon, copper and HOPG. First of all we show the data in which we compare three nitrogen bases, then data regarding different substrates is shown.

A great amount of force vs distance curves were collected, but as for adenine, only 80% of the total curves collected were to be considered analysable because of the presence of force jump during the single-molecule peeling in AFM retraction mode. Inevitably, not all the curves with a force jump were perfectly uniform for the analysis, so another data skimming was done in order to scan only a set of force vs distance curves which present the right parameters to analyze.

T [°C]	**T [K]**	**Total curves collected**	**Total curves with force jumps**	**n° of curves used for analysis**
5	278.15	4835	3868	964
10	283.15	4329	3463	945
15	288.15	6143	4914	1217
25	298.15	5476	4380	859
35	308.15	4627	3701	755
TOTAL		25410	20326	4740

Table 3: The table represent the data collected with different temperatures with a fixed loading rate of 500 nm/s.

From the above Table 3, the data achieve for the single-molecule desorption force analysis are illustrated on the histograms of Fig.3.7 where there are compared the number of force-distance curves over the desorption force for a certain temperature. The data were fitted with the help of a Gaussian's equation 2.3 which match properly for our investigation. All the graphs were scaled in x-axis from 30 pN to 110 pN to have the same model to follow without adapting the scale for each temperature.

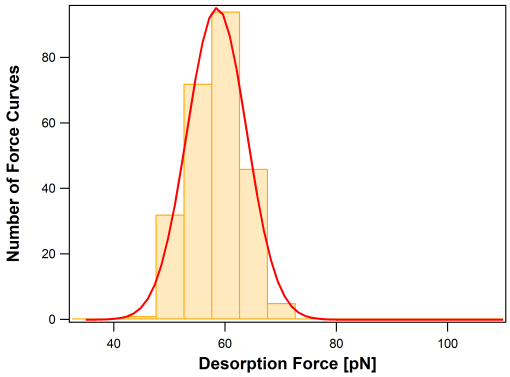

(a) Desorption Force at 5 °C

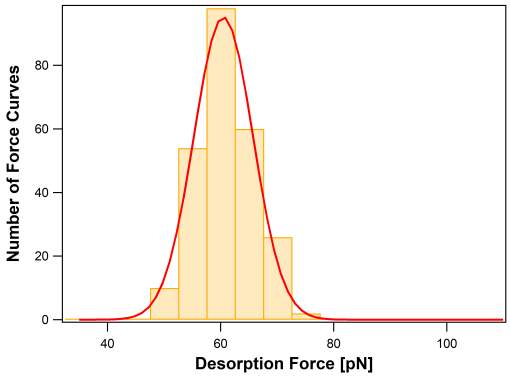

(b) Desorption Force at 10 °C

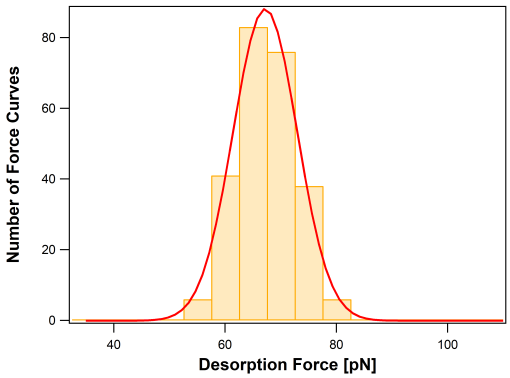

(c) Desorption Force at 15 °C

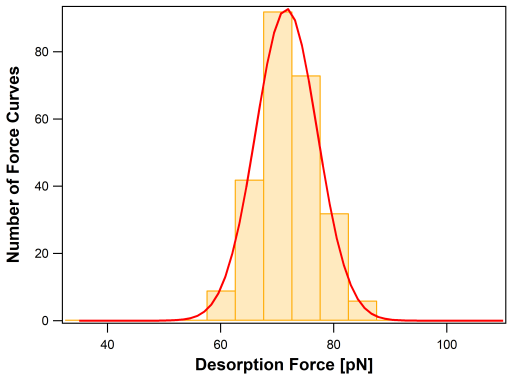

(d) Desorption Force at 25 °C

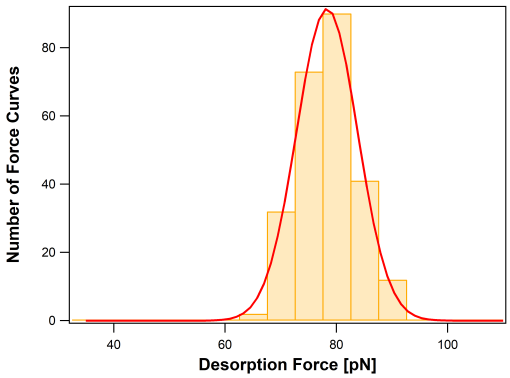

(e) Desorption Force at 35 °C

Figure 3.7: Force histograms obtained during the single-molecule force spectroscopy experiments on graphene surface. Histogram in (a) represent experiment with 5 °C environment, (b) experiment in 10 °C condition, (c) with a temperature of 15 °C, (d) at 25 °C, while (e) are data collected in 35 °C condition. The red line in all the figures is the Gaussian fitting with a formula used in equation 2.3.

The Gauss statistic is more sharp in C-homopolymers because the data obtained during the experiments were more dense for a certain range of desorption force compared to A-homopolymers where the Gauss fit is smoother and better distributed along x-axis. In the following bullet points are indicated the exact peak of desorption force for a certain number of curves and the amplitude of the peak according with the number of force vs distance curves:

- for 5 °C, 250 curves considered with desorption force peak in (56.035± 0.078) pN and a Gaussian amplitude of (95.162 ± 1.21) pN
- for 10 °C, 250 curves considered with desorption force peak in (58.011± 0.089) pN and a Gaussian amplitude of (95.16 ± 1.41) pN
- for 15 °C, 250 curves considered with desorption force peak in (64.716± 0.051) pN and a Gaussian amplitude of (88.189 ± 0.687) pN
- for 25 °C, 250 curves considered with desorption force peak in (69.159± 0.059) pN and a Gaussian amplitude of (92.787 ± 0.869) pN
- for 35 °C, 250 curves considered with desorption force peak in (75.84± 0.0623) pN and a Gaussian amplitude of (91.393 ± 0.906) pN

What we can see is that with a temperature increase, there is a change of value in the average desorption forces. This shift can tell us more about which forces dominate the peeling process under a certain conditions with a fixed loading rate. This can especially be seen once we plot graph of average desorption force dependence on temperature. To make sure that data collected is a result of data generated from the equilibrium process, we performed additional experiments where we changed the approach/retraction speed, for A-homopolymer. Velocities that were used were 500 nm/s, 200 nm/s, and 1500 nm/s. Since the loading rate experiments would take a long amount of time for all possible temperatures, for C-homopolymers we chose to change the loading rate first for condition at 25 °C and wanted to see if the average desorption force results changed dramatically from the results obtained at 500 nm/s. Since no substantial change was observed, as it is case for A-homopolymers, we decided to focus on other proprieties

and possibly describe the mechanism of the interactions, and for this reason the following table is composed of only one temperature:

T [°C]	**T [K]**	**Total curves collected with 200 nm/s**	**Total curves collected with 500 nm/s**	**Total curves collected with 1500 nm/s**
25	298.15	594	859	881

Table 4: Total curves collected with different loading rates, 200 nm/s, 500 nm/s and 1500 nm/s.

The focus was then shifted to other type of substrates in order to understand if the interaction between DNA and underlying graphene on different substrates can be affected. The substrates that were analyzed, as a substrate with monolayer graphene on top, mentioned in the first part of this section, were gold, copper, silicon and highly-oriented pyrolytic graphite (HOPG). For all these materials, experiments were performed at 25 °C condition with changes in loading rate, same as for a graphene substrate on SiO2/Si, and velocities that were used were 200 nm/s, 500 nm/s and 1500 nm/s. Only HOPG was tested without a graphene on top of it and it was made at 25 °C with a loading rate of 500 nm/s because all the other analysis concerning this particular material is well described in my mentor's article.[22] The following table represents the number of total force vs distance curves collected during the single- molecule force spectroscopy with different materials as a substrate under graphene.

Materials	**Total curves collected with 200 nm/s**	**Total curves collected with 500 nm/s**	**Total curves collected with 1500 nm/s**
Copper (Cu)	641	1209	728
Gold (Au)	738	1253	903
Silicon (Si)	580	1016	677
HOPG		656	

Table 5: Total curves collected for different graphene on substrates with different loading rates of 200 nm/s, 500 nm/s and 1500 nm/s.

From the table above there were chosen the curves which represent

faithfully the behavior of the interaction of DNA-graphene on substrate in each experiments to create histograms where the Gaussian statistics can easily match the results obtained. The histograms are shown in Fig.3.8 and the colors indicate a unique material used as a graphene holder so the reader can follow the sequence of one material histogram with criteria.

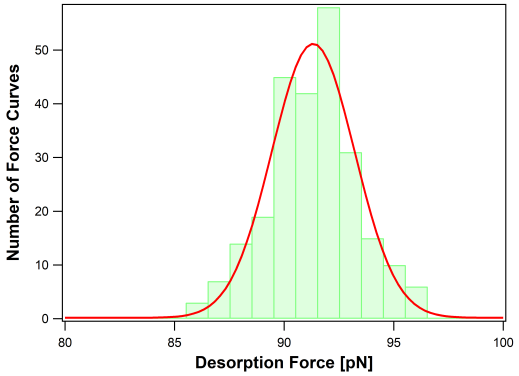

(a) Copper at 200 nm/s

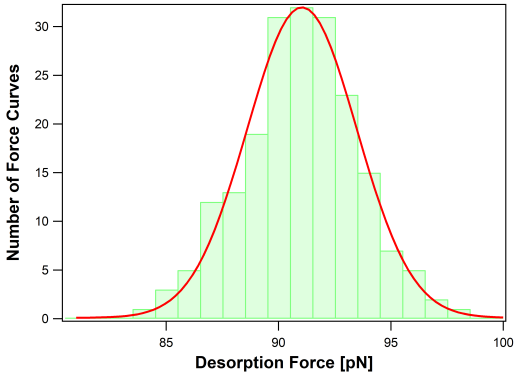

(b) Copper at 500 nm/s

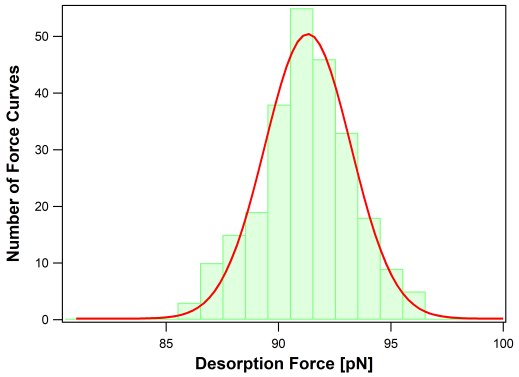

(c) Copper at 1500 nm/s

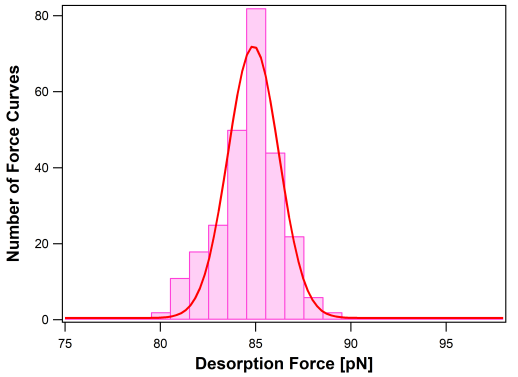

(d) Gold at 200 nm/s

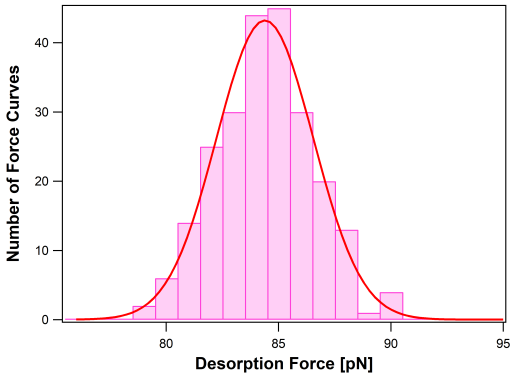

(e) Gold at 500 nm/s

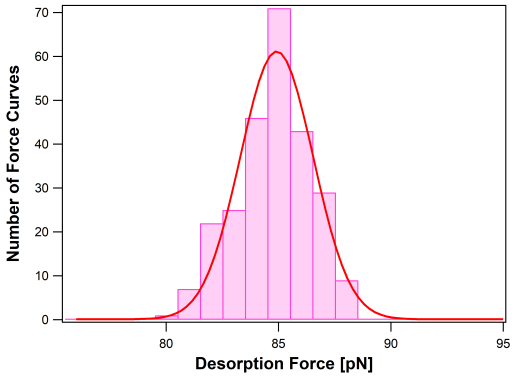

(f) Gold at 1500 nm/s

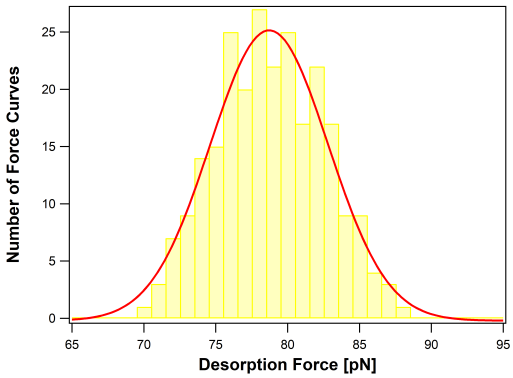

(g) Silicon at 200 nm/s

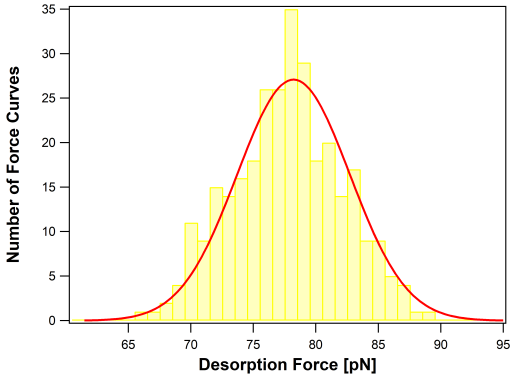

(h) Silicon at 500 nm/s

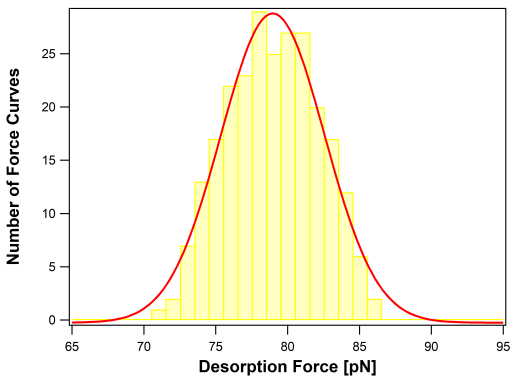

(i) Silicon at 1500 nm/s

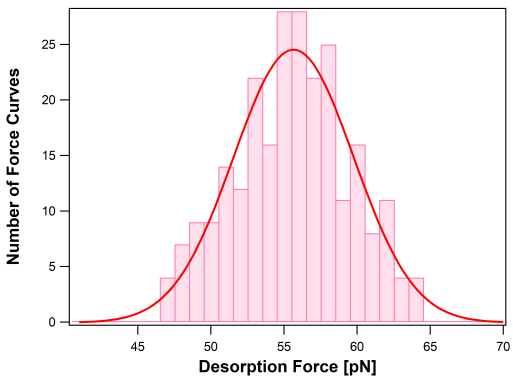

(j) HOPG at 500 nm/s

Figure 3.8: Histograms with Gaussian fit for different type of substrates at 25 °C with different loading rates. Figure (a), (b) and (c) are based on copper, images (d), (e) and (f) come from gold, while (g), (h) and (i) derive from silicon. The last image (j) corresponds to the highly-oriented pyrolytic graphite.

The core values for the analysis, as the value in picoNewton obtained for the desorption force and its relative number of force vs distance curves with the same desorption force as listed as follow for each substrates:

- Copper at 200 nm/s, 250 curves considered with desorption force peak in (90.827 ± 0.072) pN and a Gaussian amplitude of (51.021 ± 1.7) pN
- Copper at 500 nm/s, 200 curves considered with desorption force peak in (90.543 ± 0.051) pN and a Gaussian amplitude of (31.892 ± 0.571) pN
- Copper at 1500 nm/s, 251 curves considered with desorption force peak in (90.805 ± 0.048) pN and a Gaussian amplitude of (50.246 ± 1.1) pN
- Gold at 200 nm/s, 262 curves considered with desorption force peak in (84.385 ± 0.053) pN and a Gaussian amplitude of (71.546 ± 2.47) pN
- Gold at 500 nm/s, 234 curves considered with desorption force peak in (83.892 ± 0.047) pN and a Gaussian amplitude of (43.208 ± 0.826) pN
- Gold at 1500 nm/s, 253 curves considered with desorption force peak in (84.418 ± 0.059) pN and a Gaussian amplitude of (61.037 ± 1.94) pN
- Silicon at 200 nm/s, 250 curves considered with desorption force peak in (78.218 ± 0.13) pN and a Gaussian amplitude of (25.363 ± 0.725) pN
- Silicon at 500 nm/s, 305 curves considered withdesorption force peak in (77.223 ± 0.175) pN and a Gaussian amplitude of (27.101 ± 0.956) pN
- Silicon at 1500 nm/s, 250 curves considered with desorption force peak in (78.463 ± 0.079) pN and a Gaussian amplitude of (29.038 ± 0.568) pN
- Highly-oriented pyrolytic graphite (HOPG) at 500 nm/s, 250 curves considered with desorption force peak in (55.16 ± 0.186) pN and a Gaussian amplitude of (24.593 ± 1) pN

What we can see by analyzing numerical values for graphene on each substrate, by changing the loading rate, the desorption force values are not affected at all. For example, looking at the copper results for the three experiments, 200 nm/s, 500 nm/s and 1500 nm/s, the desorption force remains constant at around 90 pN. This is a great result, as it tells us that the loading rate does not affect the DNA-graphene interaction at all, so that peeling of molecules can be identified as equilibrium process. As well, for other substrates we obtain similar results and observe independence of the loading rate. I would make sense that a change in the behavior of approach/retraction curves might occur due to different material under graphene, but measurements prove otherwise. The images in Fig.3.9 represent this illustrate how the force vs distance curve can be looks depending on different material under graphene surface.

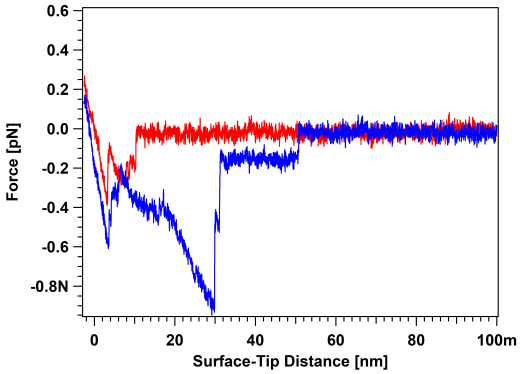

(a) Copper at 200 nm/s

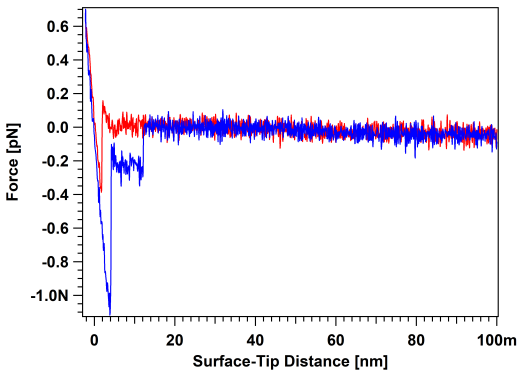

(b) Copper at 500 nm/s

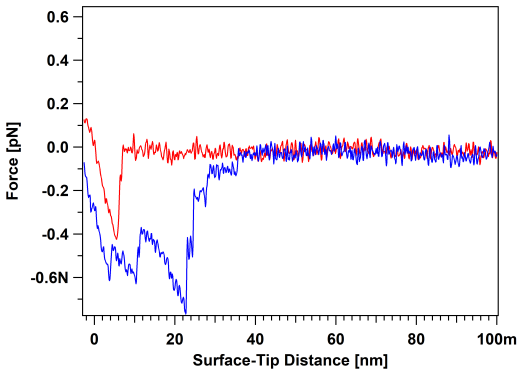

(c) Copper at 1500 nm/s

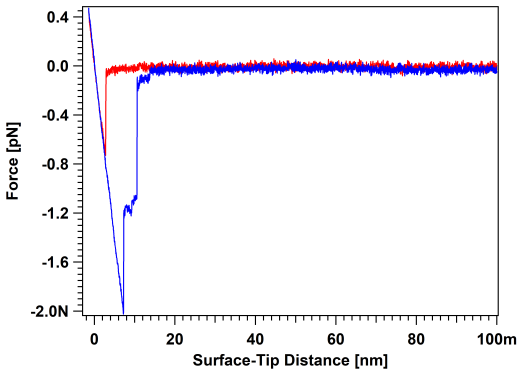

(d) Gold at 200 nm/s

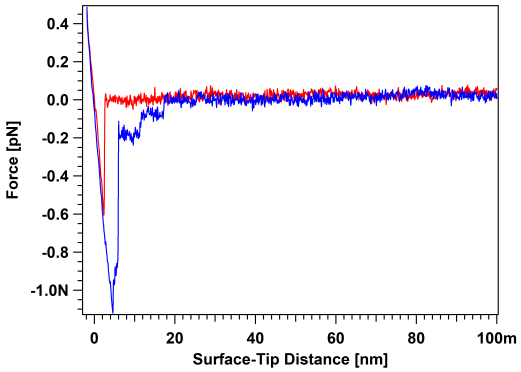

(e) Gold at 500 nm/s

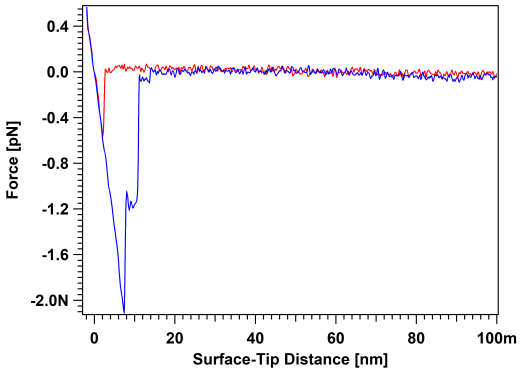

(f) Gold at 1500 nm/s

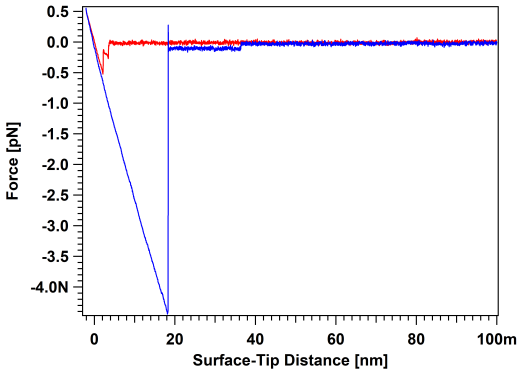

(g) Silicon at 200 nm/s

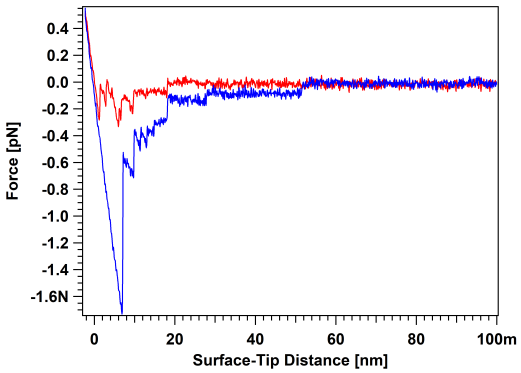

(h) Silicon at 500 nm/s

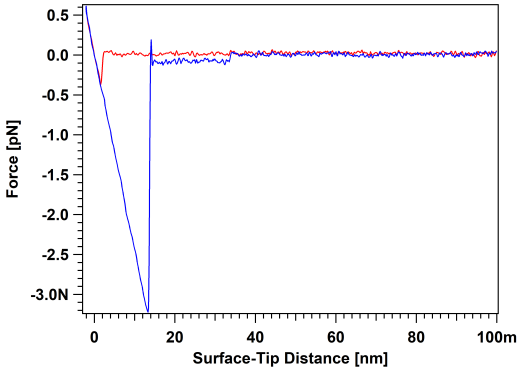

(i) Silicon at 1500 nm/s

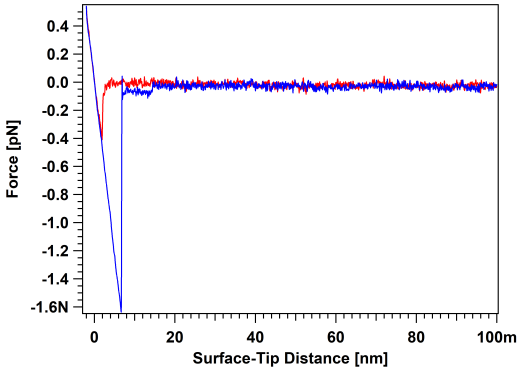

(j) HOPG at 500 nm/s

Figure 3.9: Force vs distance curves for different type of graphene substrates at 25 °C with different loading rates. Figure (a), (b) and (c) are based on copper, images (d), (e) and (f) come from gold, while (g), (h) and (i) derive from silicon. The last image (j) corresponds to the highly-oriented pyrolytic graphite.

The materials showing a behavior similar to a substrate made by SiO_2 are silicon and HOPG. These are the only two substrates that create a stable process during the approach and retraction mechanism. Surely, the behavior of HOPG is predictable because of its similar composition nature with graphene.

3.5 Nature of ss-Thymine Homopolymer Interaction with Graphene Substrate

The last homopolymer we used and analyzed was made of nucleobases called *Thymine*. It is also known as 5-methyluracil and belongs to a organic compound called hydroxypyrimidines. As well as cytosine, thymine is a nucleobase which takes a part of a pyrimidine family. This compound is made by carbon atoms (4) and nitrogen atoms (2) centered in position 1 and 3 inside the pyrimidine 6-membered ring and hydrogen atoms, as shown in Fig.3.10. The chemical formula for this nitric base is $C_5H_6N_2O_2$. Since is a pyrimidine compound, thymine has a great affinity to create a bond with the purine complementary base called adenine. In aqueous solution, free energy, enthalpy, and entropy of thymine are affected by the structuring of water around the methyl group and its difference in thermodynamic state in water is due to hydrophobic hydration at the thymine methyl.[48] In order to follow the data retrieved from Manhoar at al. thymine should possibly present a behavior in the middle of adenine and cytosine in the final force vs temperature analysis. In particular, in graphitic surface, Manhoar at al. have studied the peeling force for a polythymine molecule and they found a peeling force of 85.3 ± 4.7.[39] From this result we might think that the thymine force value should obtain a smaller value compared to adenine force value.

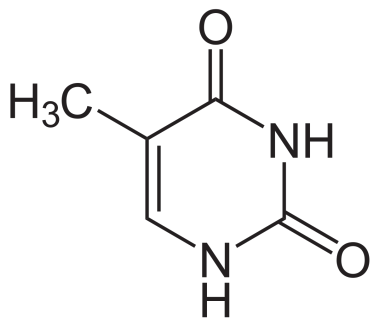

Figure 3.10: Structural representation of thymine molecule with its 6-membered ring and hydrogen bonds.

3.5.1 Data Analysis and Results

During thymine experiments, the AFM settings used were same as for adenine and cytosine. The setup had to be consistent for the three molecules in order to compare the behavior during the single molecule desorption experiments. Below there is a brief setup parameters refreshment even if all the setup details are explained in section 2.4. The compressing force between tip and surface was about 500 pN with a sampling rate of 10 kHz and low pass filter of 2 kHz. The velocity set for experiments was 500 nm/s and the temperature, as for the other two homopolymers analyzed in this thesis, changed from 5 °C up to 35 °C. The material that we analyzed was CVD grown monolayer graphene with SiO_2/Si substrate. Thymine preparation is completely explained in Chapter 2.1 where the DNA concentration is diluted from 100 μM to 0.3 nM with the right amount of thiol base solution to improve the gold-DNA bond. In order to obtain a useful amount of force vs distance curves, thymine experiments were performed consecutively during the weeks and the values shown in Table 6 indicates how difficult is to obtain appropriate force vs distance curves with a constant peeling steps. In this case, around 70 % of total curves collected were completely analyzable with a well defined force jump in retraction mode.

T [°C]	T [K]	Total curves collected	Total curves with force jumps	n° of curves used for analysis
5	278.15	4422	3228	967
10	283.15	3746	2547	1133
15	288.15	3586	2510	1041
25	298.15	5383	3606	1385
35	308.15	5209	3594	720
TOTAL		22346	15485	5246

Table 6: Number of total curves collected and analyzed for the temperature gradient with fixed loading rate of 500 nm/s

As in the previous Chapter, all the data were plotted like histogram with number of force curves vs desorption force and later fitted with Gaussian statistic. The following histograms 3.11 will show a very sharp peak around a certain values then a drop of curves near the peak. This result can be interpreted as sensitivity to a specific choice of DNA base when interact with graphene. Histograms are scaled in x-axis from 30 pN to 110 pN in order to have the same scale for each temperature.

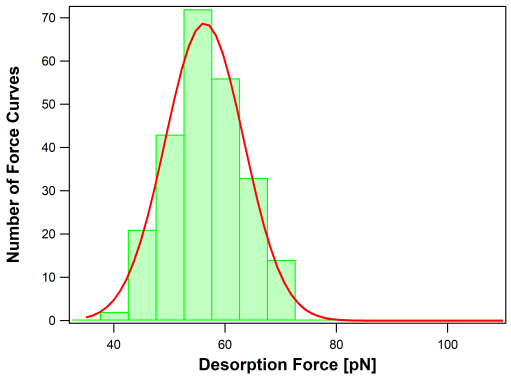

(a) Desorption Force at 5 °C

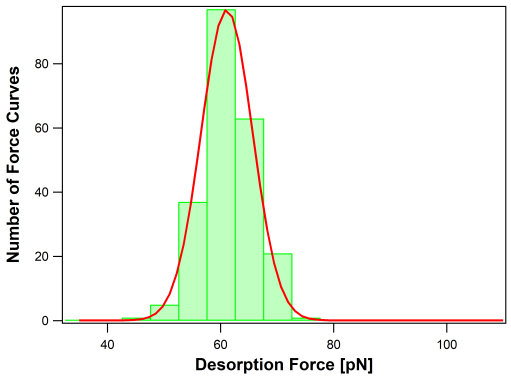

(b) Desorption Force at 10 °C

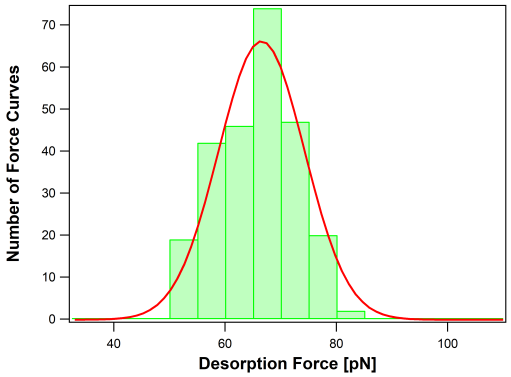

(c) Desorption Force at 15 °C

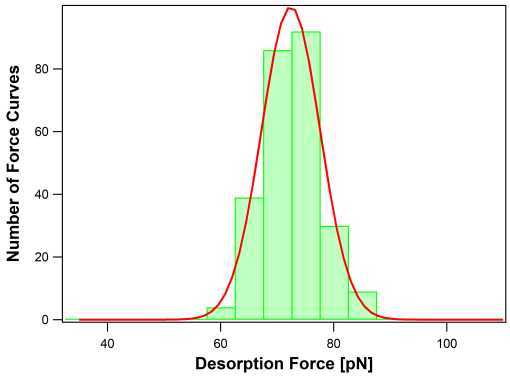

(d) Desorption Force at 25 °C

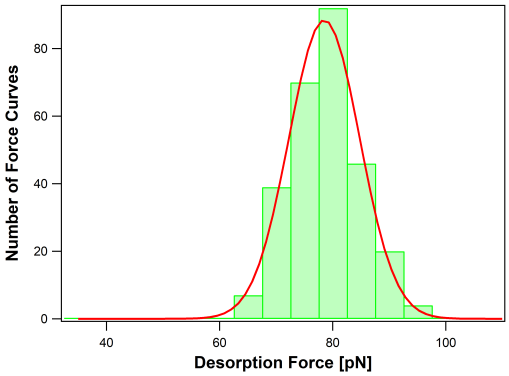

(e) Desorption Force at 35 °C

Figure 3.11: Force histograms obtained during the single-molecule force spectroscopy experiments on graphene surface. Histogram in (a) represent experiment with 5 °C environment, (b) experiment in 10 °C condition, (c) with a temperature of 15 °C, (d) at 25 °C, while (e) are data collected in 35 °C condition. The red line in all the figures is the Gaussian fitting with a formula used in equation 2.3.

The following points represent the specific values, for each temperature, concerning the position of the peak due to desorption force and the number of force curves obtained for a certain desorption force:

- for 5 °C, 241 curves considered with desorption force peak in (53.824± 0.117) pN and a Gaussian amplitude of (68.786 ± 0.992) pN
- for 10 °C, 225 curves considered with desorption force peak in (58.608± 0.068) pN and a Gaussian amplitude of (96.735 ± 1.25) pN
- for 15 °C, 250 curves considered with desorption force peak in (63.568± 0.282) pN and a Gaussian amplitude of (66.249 ± 2.11) pN

- for 25 °C, 260 curves considered with desorption force peak in (69.925± 0.068) pN and a Gaussian amplitude of (99.836 ± 1.14) pN
- for 35 °C, 278 curves considered with desorption force peak in (76.025± 0.114) pN and a Gaussian amplitude of (88.439 ± 1.41) pN

The trend of the data shows once again how the temperature affects the desorption force, indicating a smaller force value when the temperature is low, while the force increases when temperature presents a positive gradient. Experiments on thymine were conducted only in presence of 500 nm/s speed rate, without changing the loading rate parameter to higher or lower values. This policy has been adopted in order to complete the data concerning adenine, cytosine and thymine since the results obtained for the first two biological sequences have not presented any relevant considerations during loading rate modification. In Fig.3.12 are shown 3 different force vs distance curves concerning thymine tests at different temperatures, 10 °C, 25 °C and 35 °C respectively. These curves represent how meticulous has been done the data analysis, considering only curves with a clean force step during retraction process.

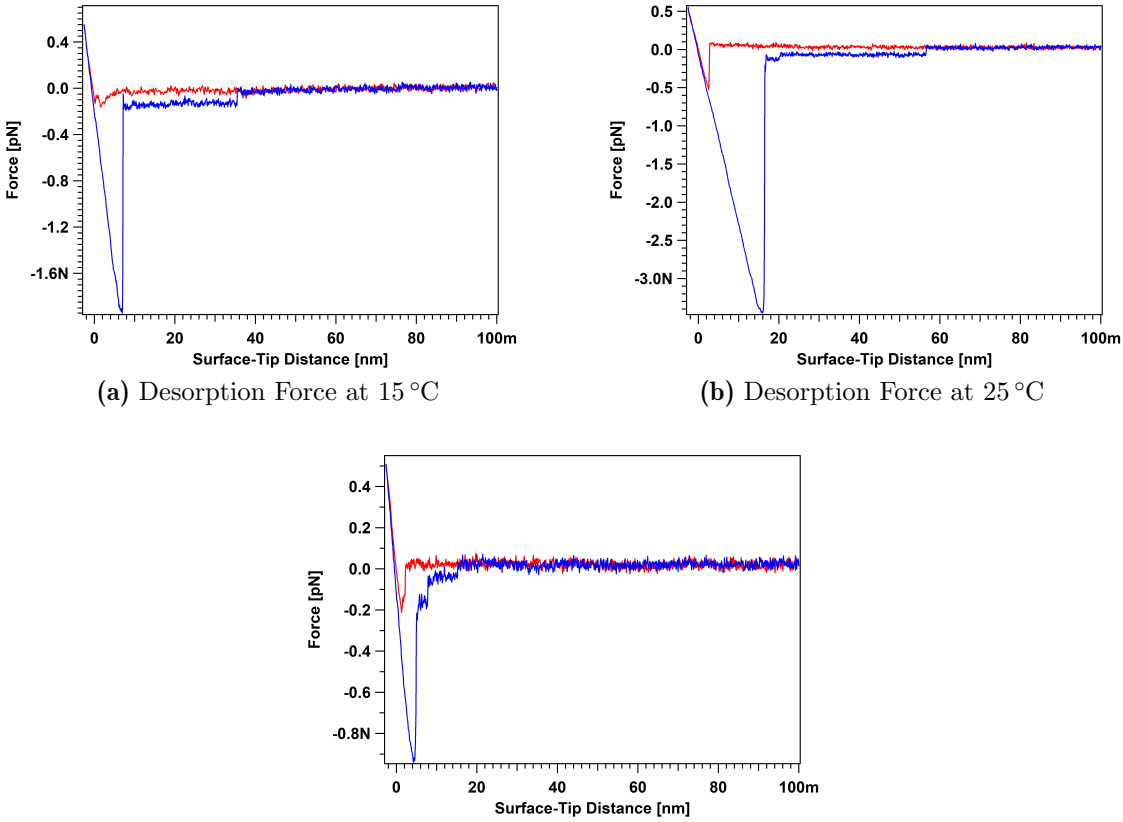

(a) Desorption Force at 15 °C

(b) Desorption Force at 25 °C

(c) Desorption Force at 35 °C

Figure 3.12: Force vs distance curves obtained during the single-molecule force spectroscopy experiments on graphene surface with thymine molecules. (a) represent experiment with 10 °C environment, (b) experiment in 25 °C condition while (c) with a temperature of 35 °C. The three curves show a flat peeling step.

3.6 Temperature Dependence in the Total Interaction

In this chapter we consider changes of temperature and its effect on force vs distance curve measurements during single molecule force spectroscopy experiments inside a liquid environment. In this kind of experiments, it is possible to get more info on the nature of interactions between DNA and underlying material. This field is still unexplored and our fundamental research can bring in new insight about very important hydrophobic interactions and pi stacking interactions of biomolecules with graphene. Once we understand how temperature affects relevant contributions in the total interaction, specific models are constructed, where we can separate individual contributions to the total interaction. For example, in literature, there are desorption force studies of ssDNA molecules from Carbon nan-

otubes. In particular, Albertorio et al.[49] have studied desorption of ssDNA molecules homopolymers (adenine, cytosine and thymine) in experiments related to thermal stability of a ssDNA-SWNT (single-wall carbon nanotube) structures, in ranges of temperatures between 4 °C - 99 °C. Their results show that desorption phenomenon is more pronounced in temperature range above 40 °C. On the other hand, when the temperature falls below 40 °C they did not notice any relevant DNA desorption. Unfortunately they did not correlate their results with hydrophobicity or any other force interactions. In nature, hydrophobic interaction is often seen as spontaneous aggregation of non-polar solutes in a polar solvent such as water, where the contact area between non-polar and surrounding polar molecules is minimized.[50,51] In order to minimize the Gibbs free energy of hydrophobic hydration, when the non-polar solute is included in a polar solvent (water), the latter molecules arrange themselves in ordered structures.[52] Moreover, hydrophobic interactions are essential in biology studies, and provide us with pivotal information regarding protein folding and unfolding.[53,54,55]

In Chapter 3.1 we introduced physical terms which represent the interfacial free energy. All values derived from equation 3.4 are useful to calculate the total interfacial free energy as a function of static contact angle, liquid surface tension, and surface energy of graphene, and DNA, respectively. All values at given temperatures are shown in Table 7. There are 2 parameters which we assume they do not change when temperature is changed, and these are: surface solid interface energy of graphene on SiO_2, also called surface energy of graphene σ_g, with value of 46.7 mJ/m^2,[56] and surface energy of DNA σ_d with value of 71 mJ/m2. Both these quantities are determined from our measurements. Considering the static contact angle α for interfacial free energy between graphene-water γ_{g-w} and inter- facial free energy between DNA-water γ_{d-w}, we separately measured graphene-water contact angle and DNA-water contact angle for a certain temperature. These parameters are shown at Fig.3.13 and the values are written in Table 7. Measured graphene-water contact angle shows a linear increase with temperature increase, while DNA-water contact angle has no particular direction of change when we change temperature from a lower to a higher temperature value and is nearly constant.

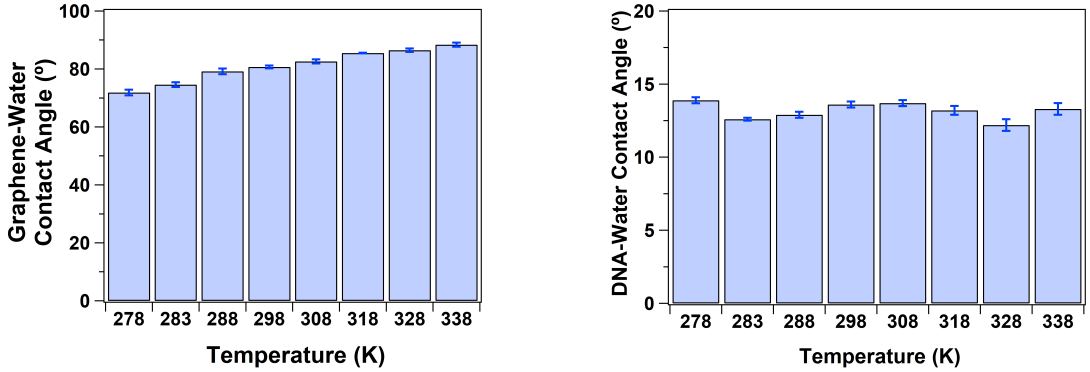

(a) Graphene-Water contact angle **(b)** DNA-Water contact angle

Figure 3.13: Representation of contact angles. (a) is the contact angle between graphene and water, while (b) is the contact angle between DNA and water.

Another parameter to take into account when temperature changes is the water tension σ_l. When temperature increases, water tension decreases linearly because distances between neighboring water molecules increase. Fig.3.14 shows behavior of water surface tension vs. temperature, together with water-air contact angle.

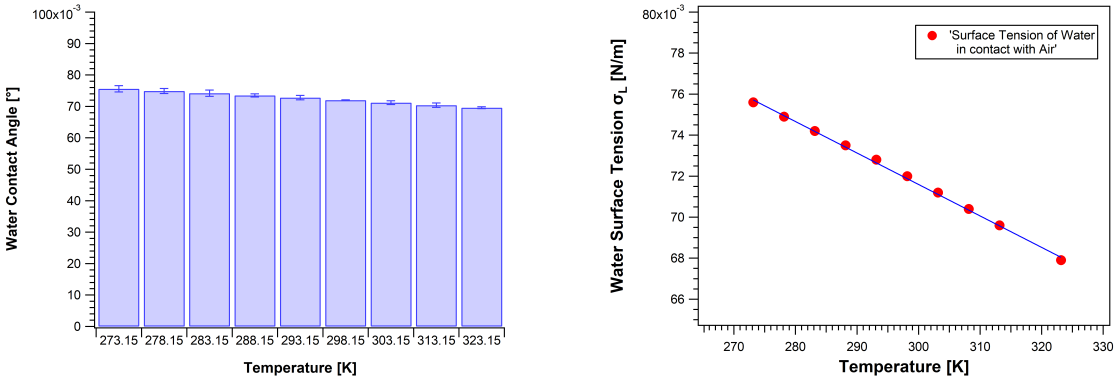

(a) Water-air contact angle **(b)** Water surface tension angle

Figure 3.14: Representation of water-air contact angle (a) and water surface tension (b), red dots, with a linear fit in blue. The y-axis for contact angle is measured in degree, while for water surface tension is measured in N/m

The terms which compose equation 3.3 are now explicitly expressed in Table 7 in order to provide to the reader a clear overview of the parameter used to calculate the total interfacial free energy in our single molecule force spectroscopy experiments.

T $[K]$	σ_d $[mJ/m^2]$	σ_g $[mJ/m^2]$	σ_l $[mN/m]$	$cos(\alpha_{d-w})$ $[^\circ]$	$cos(\alpha_{g-w})$ $[^\circ]$
278.15	71	46.7	74.9	13.9	71.9
283.15	71	46.7	74.2	12.6	74.6
288.15	71	46.7	73.5	12.9	79.2
298.15	71	46.7	72	13.6	80.7
308.15	71	46.7	70.4	13.7	82.6

γ_{g-w} $[mJ/m^2]$	γ_{d-w} $[mJ/m^2]$	$\gamma_{g-d-w}(1)$ $[mJ/m^2]$	$\gamma_{g-d-w}(2)$ $[mJ/m^2]$	$\Delta\gamma(1)$ $[mJ/m^2]$	$\Delta\gamma(2)$ $[mJ/m^2]$
23.43	-1.71	11.72	10.86	10	10.86
27	-1.41	13.5	12.8	12.09	12.79
32.93	-0.645	16.47	16.14	15.82	16.15
35.06	1.02	17.53	18.08	18.55	18.55
37.63	2.6	18.82	20.12	21.41	20.11

Table 7: Tables represent the useful parameter to deduce the total interfacial free energy of the system related with a temperature changes.

In Table 7 are illustrated all the effective values calculated to reach a total interfacial free energy. A brief reminder is below to refresh which term are involved in this study even if a complete explanation is provided in Section 3.3. γ_d is the surface energy of DNA, γ_g is the surface energy of graphene, γ_l is the liquid surface tension, α_{d-w} and α_{g-w} are the contact angle at DNA-water interface and graphene-water interface, respectively. γ_{g-w} is the interfacial energy between graphene surface and water, γ_{d-w} is the interfacial energy between DNA and water while γ_{g-d-w} is the interfacial energy when graphene-DNA-water are in contact. For the latter term, in Table 7 there are 2 formulas to take into account: the approximation formula $\gamma_{g-d-w} = \frac{1}{2} \cdot \gamma_{g-d}$ that is called $\gamma_{g-d-w}(1)$ and the complete formula $\gamma_{g-d-w} = \frac{1}{2} \cdot (\gamma_{g-w} - \gamma_{d-w})$ which is called $\gamma_{g-d-w}(2)$. These 2 formulas provide their own results in total interfacial free energy $\Delta\gamma(1)$ and $\Delta\gamma(2)$, respectively.

In Chapter 4 we will explained and showed how the desorption force of adenine, cytosine and thymine behave with changes in temperature.

We will now explore the relationship between interfacial free energy and temperature, and focus on the behavior of the three types of molecules with respect to hydrophobic and van der Waals forces, while in Chapter 5 general conclusions from measurements in this thesis project will be given.

4 Discussion and Data Comparison

In the previous Chapter 3.6 we have shown data obtained during the experiments, which were required for better comprehension of the total interfacial free energy and individual contributions to total force. Before explaining the latter results, it will be shown how the choice of basis for ssDNA strand, such as adenine, cytosine or thymine, affects interaction behavior with respect to temperature changes and compare results to each other to understand if there are significant changes during the interaction with graphene. With the help of the data analyzed in the three Chapters 3.3.1, 3.4.1 and 3.5.1, it is possible to understand the meaning of fit line slopes for each type of molecules. In addition to linear fits of our data represented we include values of given parameters with their errors.

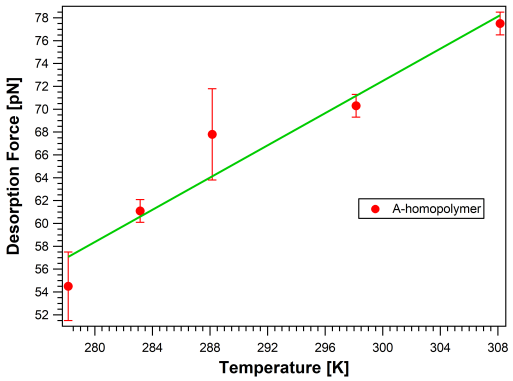

(a) Desorption Forces for A homopolymer

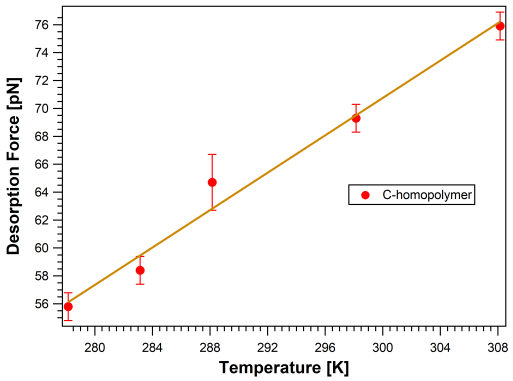

(b) Desorption Forces for C homopolymer

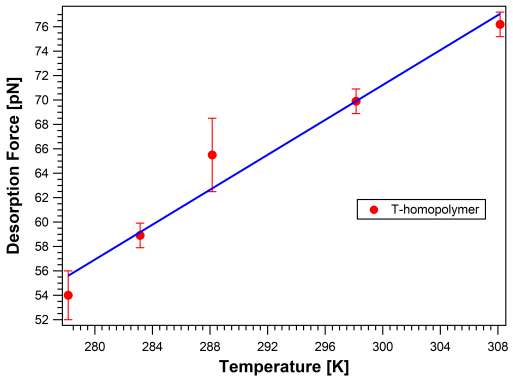

(c) Desorption Forces for T homopolymer

Figure 4.1: Graphical representation of desorption force vs temperature for the three homopolymers employed during the experiments (A, C and T) with their linear fits, green, brown and blue respectively.

Since from these individual graphs it is not simple to compare the three behaviors, the desorption forces of A, C and T were put in the same graph to see if there are variations or anomalies due to different contribution of hydrophobic forces, which would help us to build a fundamental model, and possibly exploit the numerous advantages provided by graphene and as a fruitful material for biosensing and biomedical devices.

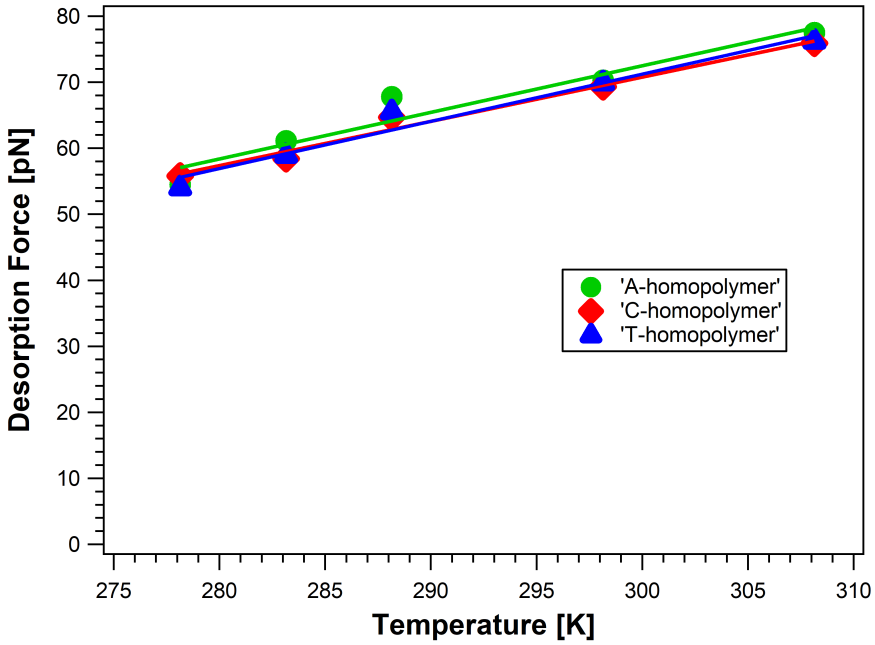

Figure 4.2: Graphical representation between the three molecules desorption force vs temperature.

Fig.4.2 compares three sets of desorption forces, adenine, cytosine and thymine homopolymers. Even though there are differences in their structures of bases, these molecules produce a similar behavior during the peeling process in different temperature environment. This is an interesting observation, especially concerning molecules hydrophobicity, and from these results it is possible to see that choice of base does not affect hydrophobic part of the interactions significantly because slopes of fit lines don't change with different choice of bases. Another comparison to make to better understand the interaction between different biological materials and graphene, is to consider the total interfacial free energy difference for each nucleobases types and comprehend how van der Waals force and hydrophobic forces are involved in interaction. In particular, to all extract these forces, it was necessary to make linear regression. Slope of the lines signifies presence of hydrophobic interactions, while intersect on y-axis in limit when total interface energy difference goes to zero. The comparison is made considering the desorption forces and the total interfacial free energy in the system.

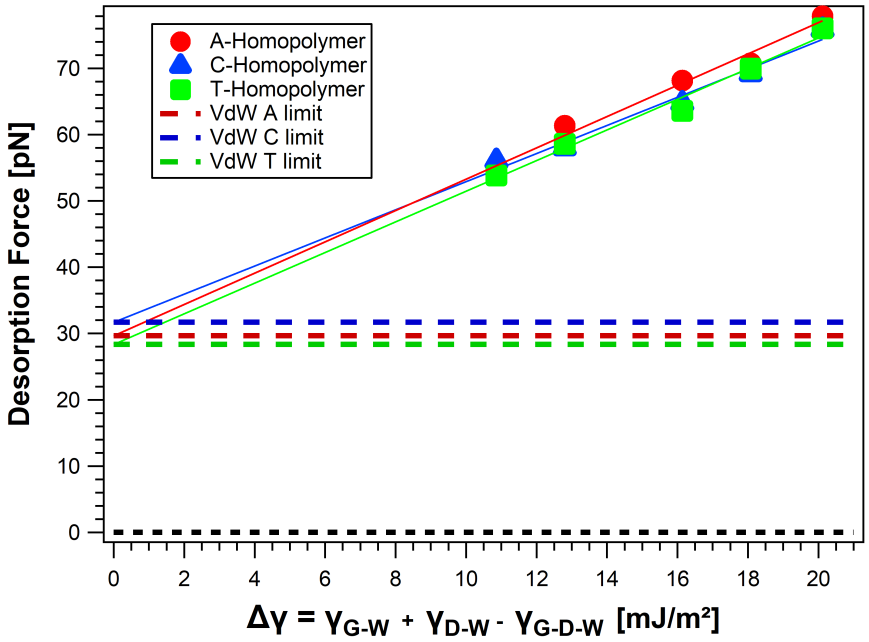

Figure 4.3: This figure represents the desorption force of A, C and T vs total interfacial free energy in the system. The dashed lines represent the limit concerning van der Waals forces, while the slopes indicate the molecule's hydrophobicity.

What can be seen from Fig.4.3, when temperature decreases total interfacial free energy decreases, and consequently also hydrophobic interactions tends to reduce. On the other hand, when total interfacial free energy $\Delta\gamma$ increases it means temperature is enhancing and also hydrophobic interactions are raising. As already seen in Chapters 3.3.1 and 3.4.1, loading rate is a parameter to take into account when dealing with single molecule force spectroscopy to understand how interactions are affected. Moreover loading rate is an important parameter to consider to understand if peeling steps are a equilibrium or non-equilibrium process. In the case of this thesis the result in Fig.4.4 show that tip velocity does not affect the peeling process and force values during experiments. For this reason, our results are in agreement with the results provided by Manohar et al. in which they claim that plateau jumps was found to be independent of loading rate.[11] The following figure shows how loading rate or loading velocities of 200 nm/s, 500 nm/s or 1500 nm/s do not compromise the desorption force values even if the material under graphene monolayer changes.

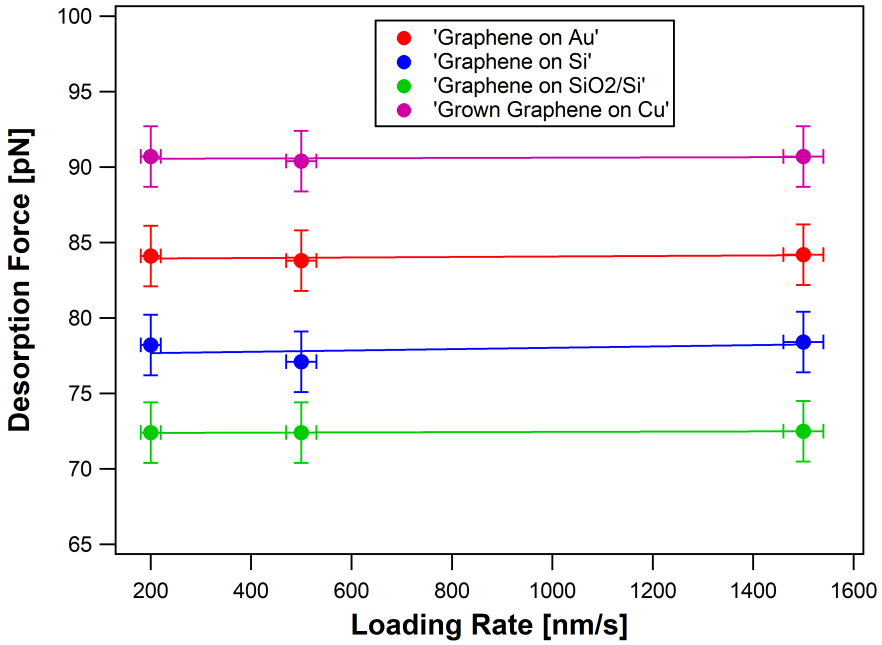

Figure 4.4: Graphical representation of desorption force vs loading rate for different graphene on substrates. It is visible how the loading rate does not affect the peeling forces.

5 Conclusion

Two dimensional materials are considered as the future of biomedical devices and biosensing in general and then they are nowadays largely investigated in single molecule detection experiments, such as nanopore DNA sequencing thanks to their mechanical robustness and excellent electronic properties. The present however, shows an inability to exploit these materials due to a lack of knowledge of their relevant interactions with DNA biomolecules, proteins and many others. Understanding this type of process can lead to more detailed knowledge and successful implementation of increasingly complex biomedical devices which contain very sensitive two dimensional sensors. In this chapter are reported conclusions about meticulous investigation of physical interactions between DNA biomolecules such as adenine, cytosine and thymine homopolymers and two dimensional monolayer graphene substrate through a careful analysis of force vs distance curves obtained with atomic force microscope. We identified and quantified the significant forces that play an essential role in total interaction. The curves collected during experiments have shown peeling of

single molecules from the surface with constant force (plateaus). These curves were statistically analyzed in order to achieve comparable results for the 3 out of 4 essential nucleobases (A, C, T), and gave us info used on the nature of interactions with graphene on SiO_2/Si and on other type of graphene supporting substrates. With the help of the literature, we concluded that the interactions in single molecule desorption forces are not electrostatic interactions, but non-electrostatic (van der Waals) and hydrophobic interactions play a dominant role during desorption process. This is an important result because gives an hint on how hydrophobic interactions are strongly involved in the total interaction. Temperature change in our experiments produced linear behavior of single molecule desorption forces with respect to temperature and total interfacial energy difference. Comparing these results with data available in literature regarding the hydrophobic interactions inside hydrophobic polymers chains at different temperature, it was deducted that with this linear behavior is a signature of hydrophobic interactions between nucleobases and hydrophobic graphene surface. Furthermore, in literature was described how supporting substrate can affect the wettability properties of the graphene layer spread over the support material. To study this phenomenon, we used different substrates such as gold, copper, silicon, silicon oxide on silicon, and freshly cleaved HOPG to support the monolayer graphene. As a result, we concluded that supporting material affect the desorption force and the desorption forces are listed as follow: $Cu > Au > SiO_2/Si > Si > HOPG$, from the highest to lowest average desorption force value. These outcomes give key interpretation on how the supporting material can tune the interaction between biomolecules and graphene. The highest desorption force results comes from metallic sup- ports and this provide an insight about how the doping of the underlying monolayer graphene can be tunable in single molecule desorption forces. These results lead us to a conjecture where the use of a specific substrate under the monolayer graphene can dramatically affect the hydrophobicity or hydrophilicity of the interaction in the system. Finally a physical analysis about the total interfacial free energy in the system was performed in order to understand if the non-electrostatic interactions can be analyzed with temperature gradient and this can be related to a change in wettability of the system such as interfacial free energy. Trying to understand if this hypothesis gives a positive result, a preliminary temperature

analysis was done in order to get some starting data, then interfacial free energy data were obtained in order to understand other mechanism behind the interaction between ssDNA and underlying graphene. In particular we needed to calculate the contact angle for graphene-water and DNA-water in order to calculate the interfacial free energy differences for graphene and DNA when they were far from each other. In the end, when all the values have been obtained, the total contribution regarding the total interfacial free energy was found and the results were ready to be compared with the data obtained from temperature analysis of desorption forces. It turned out that this two types of analysis, temperature dependence and total interfacial free energy are well correlated, because a positive change in temperature is related in a increasing value of total interfacial free energy with an enhanced value in hydrophobicity and on the other hand a negative change in total interfacial free energy produces a decrease in temperature and to a decline in hydrophobicity. Total interfacial free energy and temperature are two important parameters to understand the hydrophobicity of a single molecule desorption force system and they are needed to comprehend the trend on building the fundamental model for desorption force interactions.

6 Bibliography

References

[1] Alexander Y Grosberg; Alexei R Khokhlov. *Giant Molecules*. 1997.

[2] C Friedsam; M Seitz; H E Gaub. *Investigation of polyelectrolyte desorption by single molecule force spectroscopy*. 2004.

[3] Lulu Zhou; Mingjun Cai; Ti Tong; Hongda Wang. *Progress in the Correlative Atomic Force Microscopy and Optical Microscopy*. 2017.

[4] Hong-Qiang Li. *The Common AFM Modes*. 1997.

[5] Michel Nardin; Eugene Papirer. *Powders and Fibers: Interfacial Science and Applications*. 2006.

[6] Hendrik Hölscher; Udo D. Schwarz. *Theory of amplitude modulation atomic force microscopy with and without Q-Control*. 2007.

[7] Leo Gross; Fabian Mohn; Nikolaj Moll; Peter Liljeroth; Gerhard Meyer. *The Chemical Structure of a Molecule Resolved by Atomic Force Microscopy*. 2009.

[8] M. Paul Narchi. *Investigation of crystalline silicon solar cells at the nano-scale using scanning probe microscopy techniques*. 2016.

[9] Ramazan Asmatulu; Waseem S. Khan. *Synthesis and Applications of Electrospun Nanofibers*. 2019.

[10] John E. Sader; James W. M. Chon; Paul Mulvaney. *Calibration of rectangular atomic force microscope cantilevers*. 1999.

[11] Suresh Manohar; Amber R. Mantz; Kevin E. Bancroft; Chung-Yuen Hui; Anand Jagota; Dmitri V. Vezenov. *Peeling Single-Stranded DNA from Graphite Surface to Determine Oligonucleotide Binding Energy by Force Spectroscopy*. 2008.

[12] Efrat Roth; Alex Glick Azaria; Olga Girshevitz; Arkady Bitler; Yuval Garini. *Measuring the Conformation and Persistence Length of Single-Stranded DNA Using a DNA Origami Structure*. 1996.

[13] Dustin K. James; James M. Tour. *Graphene: Powder, Flakes, Ribbons, and Sheets*. 2012.

[14] Jungpil Kim Nodo Lee; Young Hwan Min; Seokhwan Noh; Nam-Koo Kim; Seokwon Jung; Minho Joo; Yasuhiro Yamada. *Distinguishing Zigzag and Armchair Edges on Graphene Nanoribbons by X-ray Photoelectron and Raman Spectroscopies*. 2018.

[15] Jian-Hao Chen; Chaun Jang; Shudong Xiao; Masa Ishigami; Michael S. Fuhrer. *Intrinsic and extrinsic performance limits of graphene devices on SiO2*. 2008.

[16] Akin Akturka; Neil Goldsman. *Electron transport and full-band electron-phonon interactions in graphene*. 2008.

[17] F.V. Kusmartsev; W.M. Wu; M.P. Pierpoint; K.C. Yung. *Application of Graphene within Optoelectronic Devices and Transistors*. 2014.

[18] A. H. Castro Neto; F. Guinea; N. M. R. Peres; K. S. Novoselov; A. K. Geim. *The electronic properties of graphene*. 2008.

[19] S. Ghosh; I. Calizo; D. Teweldebrhan; E. P. Pokatilov; D. L. Nika; A. A. Balandin; W. Bao; F. Miao; C. N. Lau. *Extremely high thermal conductivity of graphene: Prospects for thermal management applications in nanoelectronic circuits*. 2008.

[20] Changgu Lee; Xiaoding Wei; Jeffrey W. Kysar; James Hone. *Measurement of the Elastic Properties and Intrinsic Strength of Monolayer Graphene*. 2008.

[21] Ke Cao; Shizhe Feng; Ying Han; Libo Gao; Thuc Hue Ly; Zhiping Xu; Yang Lu. *Elastic straining of free-standing monolayer graphene*. 2020.

[22] Milan Blaskovic; Slaven Garaj. *Single-molecule study of interaction between DNA molecules and 2D materials*. 2018.

[23] Francesca Iacopi; John J. Boeckl; Chennupati Jagadish. *Semiconductor and Semimetals vol.95*. 2016.

[24] Liuyang Zhang; Xianqiao Wang. *DNA Sequencing by Hexagonal Boron Nitride Nanopore: A Computational Study*. 2016.

[25] Katsuyoshi Kobayashi; Jun Yamauchi. *Electronic structure and scanning-tunneling-microscopy image of molybdenum dichalcogenide surfaces*. 1995.

[26] Amir Barati Farimani; Kyoungmin Min; Narayana R. Aluru. *DNA Base Detection Using a Single-Layer MoS2*. 2014.

[27] Suresh Manohar; Amber R Mantz; Kevin E Bancroft; Chung-Yuen Hui; Anand Jagota; Dmitri V Vezenov. *Peeling Single-Stranded DNA From Graphite Surface to Determine Oligonucleotide Binding Energy by Force Spectroscopy*. 2008.

[28] Fujihira M; Okabe Y; Tani Y; Furugori M; Akiba U. *A novel cleaning method of gold-coated atomic force microscope tips for their chemical modification*. 2000.

[29] Tonya M. Herne; Michael J. Tarlov. *Characterization of DNA Probes Immobilized on Gold Surfaces*. 1997.

[30] Rastislav Levicky; Tonya M. Herne; Michael J. Tarlov; Sushil K. Satija. *Using Self-Assembly To Control the Structure of DNA Monolayers on Gold: A Neutron Reflectivity Study*. 1998.

[31] Sirnegeda D. Techane; Lara J. Gamble; David G. Castner. *Multitechnique Characterization of Self-Assembled Carboxylic Acid-Terminated Alkanethiol Monolayers on Nanoparticle and Flat Gold Surfaces*. 2011.

[32] Xuelei Liang; Brent A. Sperling; Irene Calizo; Guangjun Cheng; Christina Ann Hacker; Qin Zhang; Yaw Obeng; Kai Yan; Hailin Peng; Qiliang Li; Xiaoxiao Zhu; Hui Yuan; Angela R. Hight Walker; Zhongfan Liu; Lian mao Peng; Curt A. Richter. *Toward Clean and Crackless Transfer of Graphene*. 2011.

[33] X. D. Zhou; S. C. Zhang; W. Huebner; P. D. Ownby; Hongchen Gu. *Effect of the solvent on the particle morphology of spray dried PMMA*. 2011.

[34] Mona M. M. Alyobi; Chris J. Barnett; Richard J. Cobley. *Effects of Thermal Annealing on the Properties of Mechanically Exfoliated Suspended and On-Substrate Few-Layer Graphene*. 2017.

[35] A. Misra; S. Sharma; T. Acosta; J. Porter; D. Bates. *Single-Pulse Standoff Raman Detection of Chemicals from 120 m Distance during Daytime*. 2012.

[36] Derek J. Gardiner and Pierre R. Graves. *Practical Raman Spectroscopy*. 1989.

[37] L.M.Malard; M.A.Pimenta; G.Dresselhaus; M.S.Dresselhaus. *Raman spectroscopy in graphene*. 2009.

[38] Andrea C. Ferrari and Denis M. Basko. *Raman spectroscopy as a versatile tool for studying the properties of graphene*. 2013.

[39] Sara Iliafar; Kyle Wagner; Suresh Manohar; Anand Jagota and Dmitri Vezenov. *Quantifying Interactions between DNA Oligomers and Graphite Surface Using Single Molecule Force Spectroscopy*. 2012.

[40] Sara Iliafar; Jeetain Mittal; Dmitri Vezenov and Anand Jagota. *Interaction of Single-Stranded DNA with Curved Carbon Nanotube Is Much Stronger Than with Flat Graphite*. 2014.

[41] Chelsea R. Martinez and Brent L. Iverson. *Rethinking the term "pi-stacking"*. 2012.

[42] Yukihiro Yonemoto and Tomoaki Kunugi. *Wettability model for various-sized droplets on solid surfaces*. 2014.

[43] Andrew Kozbial; Zhiting Li; Caitlyn Conaway; Rebecca McGinley; Shonali Dhingra; Vahid Vahdat; Feng Zhou; Brian D'Urso; Haitao Liu and Lei Li. *Study on the surface energy of graphene by contact angle measurements*. 2014.

[44] D. K. Owens and R. C. Wendt. *Estimation of the surface free energy of polymers*. 1969.

[45] Lasse Makkonen. *Young's equation revisited*. 2016.

[46] Lakna Panawala. *Difference Between Purines and Pyrimidines Difference Between Purines and Pyrimidines*. 2017.

[47] Robert M. Elder and Arthi Jayaraman. *Structure and thermodynamics of ssDNA oligomers near hydrophobic and hydrophilic surfaces*. 2013.

[48] J. N. Spencer and T. A. Judge. *Hydrophobic Hydration of Thymine*. 1983.

[49] Fernando Albertorio; Mary E. Hughes; Jene A. Golovchenko and Daniel Branton. *Base dependent DNA-carbon nanotube interactions: activation enthalpies and assembly-disassembly control*. 2009.

[50] Charles Tanford. *Contribution of Hydrophobic Interactions to the Stability of the Globular Conformation of Proteins*. 1962.

[51] R L Baldwin. *Temperature dependence of the hydrophobic interaction in protein folding*. 1986.

[52] Isaac T. S. Li and Gilbert C. Walker. *Signature of hydrophobic hydration in a single polymer*. 2011.

[53] Isaac T. S. Li and Gilbert C. Walker. *Single Polymer Studies of Hydrophobic Hydration*. 2012.

[54] Isaac T. S. Li and Gilbert C. Walker. *Interfacial Free Energy Governs Single Polystyrene Chain Collapse in Water and Aqueous Solutions*. 2010.

[55] Emily E. Meyer; Kenneth J. Rosenberg and Jacob Israelachvili. *Recent progress in understanding hydrophobic interactions*. 2006.

[56] Shiren Wang; Yue Zhang; Noureddine Abidi and Luis Cabrales. *Wettability and Surface Free Energy of Graphene Films*. 2009.

Acknowledgments

First of all, the biggest thanks goes to my family and my girlfriend who supported and encouraged me for the duration of this master's degree. Due to their endless love I managed to overcome all the obstacles along this path. Even if they were miles away, it is like they have been always by my side. In details, I want to thank my mom Enrica Pachera and my dad Andrea Alberti because they have never made me miss anything and have taught me all the principles and vicissitudes that have made me the man I am today, to face life in the best way possible. To my brother Saverio and his wonderful family, whom I love from the soul and who enriched this path with excellent advice and moral support. An immense thank you to my girlfriend Letizia because she was my backbone for all this period. Without her capability of reflection, understanding and patience I would not be able to conclude this difficult path. I also want to thank her for all the times we only had to see each other for a few hours or even for having been patient for weeks and months without seeing each other. She, together with my family, were the strengths of my journey and I am really proud that they are part of my life. A heartfelt thanks to Letizia's family who made me feel at home every time and my grandmother Bruna and all my aunts, uncles and cousins. Despite the distance, I want to thank my friends Alessandra, Erica e Marco who made me feel like I wasn't far away.

A strong thank you goes to Prof. Slaven Garaj and Dr. Milan Blaskovic for giving me the opportunity to work on this thesis project and for teaching me many facets of working in a research environment as important as NUS. I would like to thank Dr. Massimo Spina which allowed me to embark on a wonderful experience in Singapore, by giving me inspiring advice and guiding me to wonderful places in this state. As well, I would like to thank to all NUS staff, especially to people from Physics Department which were friendly, supportive and considerate towards me. I would also like to add all the people from Centre for Advanced 2D materials into this list because they were knowledgeable, friendly, and fun to spend time with.

An unfailing thanks to all the professors of this Nanotechnologies for ICTs study who taught me very interesting subjects by stimulating my knowledge and allowing me to know and visit different cities and cultures such as Turin, Grenoble, Lausanne, Zurich and Singapore. A heartfelt thanks to my professor and supervisor Matteo Cocuzza for his clarity of teaching during the semesters in Turin and Grenoble, willingness to help us students in every situation and for having had understanding words in delicate moments of the path.

A big thank you to my companions in adventure and misadventure Bruno Brajon, Dario Bonincontro, Davide Tosolini, Ernesto Gribaudo, Leo Poitrimolt and Tommaso Milanese. We shared unforgettable and funny moments, in the three cities that hosted us, and on the other hands we went through some very tough and intense period of study.